Gina Cody School of Engineering and Computer Science

Department of Electrical and Computer Engineering

Hybrid Precoding in Millimeter-Wave Massive MIMO Systems with Deep Learning

Pranav Jha

Student ID: 40081750

Ph.D. Comprehensive Examination Report

Supervisor

Dr. Wei-Ping Zhu

January 2020

Abstract: Millimeter-wave (mm-Wave) multiple input multiple output (MIMO) has been considered as a promising technique in improving the overall throughput of the future 5G wireless networks due to the large available bandwidth in mm-Wave spectrum ((30 GHz-300 GHz)) and higher spectrum efficiency of massive MIMO systems. However, mm-Wave signals suffer from free-space path loss and require sufficient antenna array gain or beamforming gain to minimize this effect. The array gain can be achieved by precoding (beamforming) in massive MIMO systems with large antenna array which provides higher multi-user gain and establish links with reasonable signal-to-noise ratio (SNR). On the other hand, mm-Wave signals enable such large antenna array in massive MIMO to be packed in small physical dimension. For MIMO, conventionally, precoding is done in baseband, however, due to the baseband hardware complexity and power consumption related to the mixed analog-to-digital components (ADCs), digital precoding is prohibitive in mm-Wave massive MIMO systems. Analog beamforming is relatively simple but limited by the availability of only quantized phase shifters (PSs) with constant amplitudes. This makes hybrid precoding where the precoder processing is divided between analog and digital domains, a promising solution in mm-Wave massive MIMO systems.

In this regard, this report investigates the hybrid precoding techniques in the mm-Wave massive MIMO systems through two key papers and the references therein. In the first paper [1], for the mm-Wave massive MIMO system with large antenna array, a successive interference cancellation (SIC)-based hybrid precoding is proposed. In contrast to most hybrid precoding techniques, where a fully-connected architecture is considered for hybrid precoding, this proposed technique considers a sub-connected architecture. Unlike the fully-connected architecture where the number of RF chains is the same as the number of antennas, this sub-connected architecture uses less number of RF chains as compared to the number of antennas to increase the energy efficiency of the ADCs. This technique achieves a near-optimal performance with low complexity. In the second paper [2], a deep learning (DL) based framework is developed to reduce the high computational complexity in hybrid precoding of mm-Wave massive MIMO system which exploits the sparsity present in mm-Wave signals. The complexity of these approaches are compared to the hybrid precoding based on spatially sparse precoding proposed in [3] where by exploiting the spatial structure of mm-Wave channels, precoding/combining is formulated as a sparse reconstruction problem. In both the papers, two different approaches have been used to improve the energy efficiency and to reduce the computational-complexity involved in the hybrid precoding of mm-Wave massive MIMO systems. This report ends with highlighting the limitations of the work discussed in both the papers and provide insight towards potential future direction of this research.

Contents

1 Introduction

1.1 Dawn of Millimeter-Wave Massive MIMO

Mm-Wave massive MIMO is a promising candidate technology for exploring new frontiers for future 5G networks. It benefits from the combination of large available bandwidth in mm-Wave frequency bands and high antenna gains achievable with massive MIMO antenna arrays. With enhanced energy and spectral efficiencies, increased reliability, compactness, flexibility and improved overall system capacity, mm-Wave massive MIMO is expected to address the challenges of the explosively growing mobile data demand. For mm-Wave massive MIMO systems, maximum benefits can be achieved when different transceiver antenna pairs experience independently fading channel coefficients. This is realizable when the antenna element's spacing is at least 0.5λ, where λ is the wavelength of the signal. Since λ reduces with increasing carrier frequency, a higher number of elements in antenna arrays of same physical dimension can be realized at mm-Wave than at μ-Wave frequencies. The realization of this optimal performance is dependent on the availability of accurate channel state information (CSI). At mm-Wave frequencies, the dimensions of antenna elements as well as the inter-antenna spacing become incredibly small due to their dependence on wavelength. This makes possible to pack a large number of antenna elements in a physically limited space, thereby enabling massive MIMO antenna array, not only at the base stations (BSs) but also at the user equipments (UEs) [4].

In mm-Wave communication, signals propagated at mm-Wave frequencies experience higher pathloss with increasing frequency and have lesser penetrating power through solids and buildings, thereby making them significantly more prone to the effects of shadowing, diffraction and blockage, as the wavelength is typically less than the physical dimensions of the obstacles [5, 6]. However, the smaller wavelength which enables massive antenna arrays and the huge available bandwidth in the bands can compensate for the losses to maintain and even drastically boost performance gains with respect to spectral and energy efficiencies, provided evolving computational complexity, signal processing, and other implementation issues are addressed.

1.2 Millimeter-Wave Massive MIMO System Model

1.2.1 Antenna Array

In MIMO systems, generally, beamforming is being used to improve the performance of wireless links in terms of achievable throughput. There are three types of antenna array architecture that have evolved over time as fully-digital, fully-analog, and hybrid analog-digital architecture. A fully-digital implementation employs dedicated RF front-end and digital baseband per antenna, which for the mm-Wave massive MIMO is prohibitively costly and practically infeasible due to tight space constraints. The fully-analog array, on the other hand, uses only one RF chain with multiple analog phase shifters (PSs). It has simple hardware structure but suffers from poor system performance. Also, it has low antenna gain, as only the phases of the signals, but not their amplitudes can be controlled.

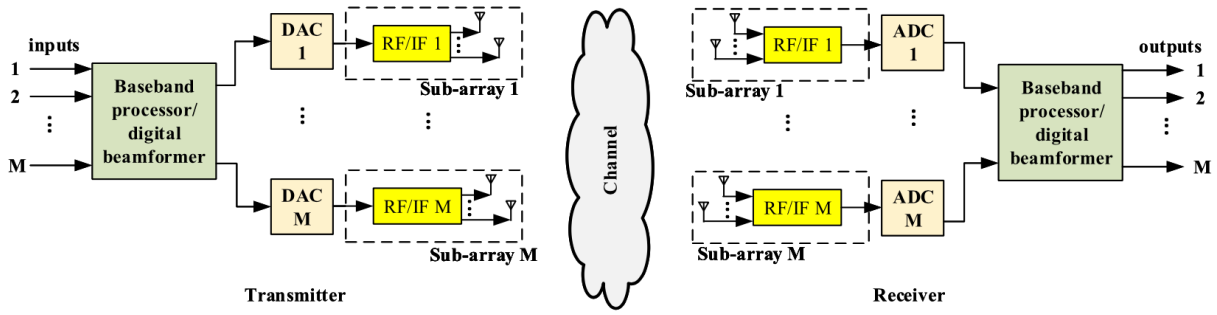

Figure 1: Architecture of hybrid antenna array system.

The more feasible and practical approach, according to research trends, is the massive hybrid array which consists of multiple analog sub-arrays with their own respective digital chains [7]. In the massive hybrid array architecture, antenna elements are grouped into analog sub-arrays. Only one PS is dedicated to a single antenna element and all other components are shared by all antenna elements in each sub-array. Each sub-array is fed with only one digital input and outputs only one digital signal, and all digital signals from all the sub-arrays are jointly processed in a digital processor. Overall, this hybrid structure, shown in Fig. 1 [4], significantly reduces the cost, number of required hardware components and system complexity, and the performance is roughly comparable with the optimal but costly and unfeasible fully-digital architecture [1].

In terms of structure, antenna arrays are typically designed as either uniform linear array

(ULA) or uniform planar array (UPA). The array response vector for the uniform linear array (ULA) with U elements, which is independent of the elevation angle, is given as

$$\mathbf{f}_{\mathrm{ULA}}(\phi) = \frac{1}{\sqrt{U}}\left[1, e^{j\frac{2\pi}{\lambda}d\sin(\phi)}, \ldots, e^{j(U-1)\frac{2\pi}{\lambda}d\sin(\phi)}\right]^T. \quad (1)$$

where λ is the wavelength of the signal and d is the antenna spacing. In addition, the array response vector for uniform planar array (UPA) with W_1 and W_2 elements on horizontal and vertical, respectively is given as

$$\mathbf{f}_{\mathrm{UPA}}(\phi,\theta) = \frac{1}{\sqrt{U}}\left[1, \ldots, e^{j\frac{2\pi}{\lambda}d(x\sin(\phi)\sin(\theta)+y\cos(\theta))}, \ldots, e^{j\frac{2\pi}{\lambda}d((W_1-1)\sin(\phi)\sin(\theta)+(W_2-1)\cos(\theta))}\right]^T, \quad (2)$$

where $0 \leq x \leq (W_1 - 1)$ and $0 \leq y \leq (W_2 - 1)$. Considering UPAs are of interest in mm-Wave beamforming because they (1) yield smaller antenna array dimensions; (2) facilitate packing more antenna elements in a reasonably sized array; and (3) enable beamforming in the elevation domain (also known as 3D beamforming) [7].

1.2.2 Channel Model

The high free-space path loss is a characteristic of mm-Wave propagation, leading to limited spatial selectivity or scattering. On the other hand, the large tightly packed antenna arrays are characteristics of mm-Wave transceivers, leading to high levels of antenna correlation. This feature of tightly packed arrays in sparse scattering environments makes many of the statistical fading distributions used in traditional MIMO analysis inaccurate for mm-Wave channel modeling [7]. For this reason, a narrow-band channel representation, based on the Saleh-Valenzuela model has been considered, which allows to accurately capture characteristics in mm-Wave channels. Using this channel model, the channel matrix H is assumed to be a sum of the contributions of L propagation paths. Therefore, the discrete-time narrow-band channel H can be written as

$$\mathbf{H} = \gamma \sum_{l=1}^{L} \alpha_l \Lambda_r(\phi_l^r, \theta_l^r)\Lambda_t(\phi_l^t, \theta_l^t)\mathbf{f}_r(\phi_l^r, \theta_l^r)\mathbf{f}_t^H(\phi_l^t, \theta_l^t), \quad (3)$$

where $\gamma = \sqrt{\frac{NMK}{L}}$ represents the normalization factor, L represents the limited number of scatters where $L \leq N$ for mm-Wave communication systems. $\alpha_l \in \mathbb{C}$ represents the gain of l-th path. $\phi_l^t(\theta_l^t)$ and $\phi_l^r(\theta_l^r)$ represent the azimuth angles of departure and arrival (AoDs/AoAs), respectively. $\Lambda_t(\phi_l^t, \theta_l^t)$ and $\Lambda_r(\phi_l^r, \theta_l^r)$ represent the transmit and receive antenna array gain at a specific AoD and AoA, respectively. $\mathbf{f}_r(\phi_l^r, \theta_l^r)$ and $\mathbf{f}_t^H(\phi_l^t, \theta_l^t)$ represent the antenna array response vectors depending on the antenna array structures at the BS and the the user, respectively.

1.2.3 Precoding Techniques

The design of precoding schemes is highly essential for mm-Wave massive MIMO cellular systems. Precoders optimize the performance of mobile networks using the concept of interference cancellation in advance, by controlling the phases and/or amplitudes of original signals. This process is also known as beamforming. Precoding schemes can generally be classified into three categories as analog beamforming, digital precoding and hybrid (analog-digital) precoding.

Analog beamforming: While analog beamforming is used to control the phases of signals with the single data stream in order to realize optimal antenna array gain and effective SNR, it can only be employed for single-stream single-user systems. It requires only one RF chain, which makes it easier to be implemented, however, analog beamforming usually suffers from serious performance loss, since only the phases of the transmit signals can be controlled.

Digital precoding: Digital precoding is a traditional technology widely used in low-frequency MIMO systems. The basic idea of digital precoding is to control both the phases and amplitudes of original signals to cancel interferences in advance. Digital precoding schemes are classified as either linear, where the transmitted signals are composed by a linear combination of the original signals or non-linear, where the transmitted signals are obtained in a nonlinear way.

Hybrid precoding: This is a promising scheme for mmWave massive MIMO networks as it offers a significant reduction in the number of required RF chains and the associated energy consumption and cost when compared with digital precoding, yet achieving near-optimal performance. It realizes this hybrid configuration by employing a small-size digital precoder with a small number of RF chains to cancel interference in the first step, and a large-size analog beamformer with a large number of only phase shifters without RF chains in the second step to increase

the antenna array gain [7]. For a single-user system, hybrid precoders can be grouped into two structural classes: (i) the fully connected architecture, where each RF chain is connected to all BS antennas via PSs, example is the spatially-sparse hybrid precoder, proposed in [3] (ii) the subconnected architecture, where each RF chain is connected to only a subset of BS antennas, example is the successive interference cancellation (SIC)-based hybrid precoder, proposed in [1], as shown in Figs. 2 and 3 [1], respectively and discussed below .

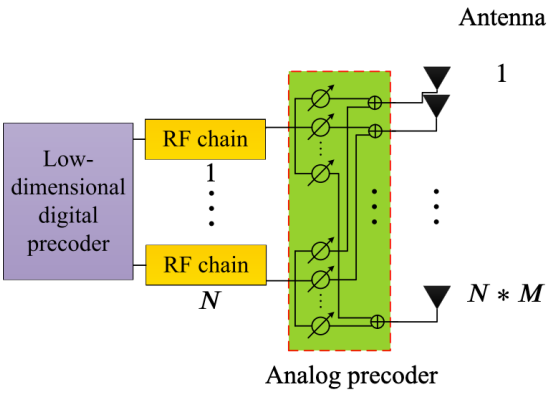

Figure 2: Fully-connected architecture

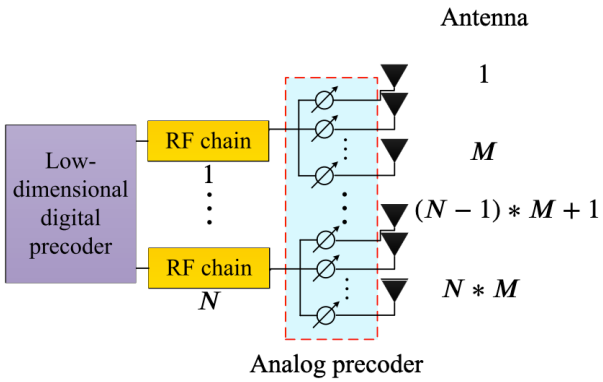

Figure 3: Sub-connected architecture

1. Fully-connected architecture: This is shown in Fig. 2 [1], where the number of radio-frequency (RF) chains is N and the number of total antenna elements is NM. It can be seen that the transmitted signal on each of the N digital RF chains goes through NM RF paths and summed up before being connected with each of the NM antenna elements. Analog precoding is performed over NM RF paths for each RF chain and digital precoding can then be performed over N RF chains. This structure is a natural combination of analog orecoder and digital precoder which acheives full precoding gain for each RF chain. However the complexity of this structure is high as the total number of RF paths is N^2M.

2. Sub-connected architecture: This is shown in Fig. 3 [1], where each of the N RF chain is connected to only a subset M of NM antennas. In this case, digital precoding is performed over N RF chains and analog precoding is performed only over M RF paths for each RF chain. This architecture is suitable for the deployment of antenna elements in base station for current cellular systems, where each RF chain is generally connected to a column of antenna elements. Compared to the fully-connected architecture, the precoding gain for each RF chain in a sub-connected architecture reduces by a factor of $1/N$, however, the complexity also get reduced by $1/N$ as

the total number of RF paths is only NM. This shows that the fully-connected architecture can achieve higher spectrum efficiency, while the sub-connected architecture is expected to achieve higher energy efficiency as it requires less number of PSs [8].

2 Literature Review

While the fundamentals of precoding (beamforming) are the same regardless of carrier frequency, signal processing in mm-Wave massive MIMO systems is subject to a set of nontrivial practical constraints [9]. The analog beamforming for mm-Wave communications is realized by the phase shifters (PSs) and a small number of RF chains, which places constant amplitude constraints on the design of the analog beamformer [10]. These constraints cause performance loss, although it is simple to be implemented in the hardware. In digital precoding, the need of a dedicated baseband and RF chain for each antenna element makes the system costly and energy-intensive. If digital precoding is directly applied in mm-Wave massive MIMO systems with a large antenna array, the high number of RF chains will high cost and energy consumption. For example, the energy consumption of one RF chain (including digital-to-analog converter, up converter, etc.) at mm-Wave is about 250 mW [10], and for a mm-Wave massive MIMO system with 64 antennas, 16 W will be consumed just by RF chains, not to mention the transmitted energy. To solve this problem, the hybrid analog and digital precoding is proposed in [3] which exploits the spatial structure of mm-Wave channels and formulated precoding/combining problem as a sparse reconstruction problem, and also develops a precoding algorithm to accurately approximate optimal unconstrained precoder and combiner with low-cost RF hardware. Specifically, it divides the optimal digital precoder into two steps. In the first step, a small-size digital precoder (realized by a small number of RF chains) is employed to cancel interferences, while in the second step, a large-size analog beamformer (realized by a large number of analog phase shifters without RF chains) is used to increase the antenna array gain. Therefore, hybrid precoding can significantly reduce the number of required RF chains without obvious performance loss, which makes it a promising precoding technology for mm-Wave massive MIMO systems.

In other words, the spatially sparse precoding is to formulate the sum-rate optimization prob-

lem as a sparse approximation problem. Then, classical algorithms in sparse signal recovery, such as OMP algorithm, can be utilized. This algorithm takes an optimal unconstrained precoder as input, and approximates it as a linear combination of beam steering vectors that can be applied by analog circuitry together with a digital precoder at baseband to obtain the near-optimal practical hybrid precoder. Simulation results show that for typical mm-Wave massive MIMO systems, the spatially sparse hybrid precoding can achieve a performance quite close to the optimal unconstrained precoder, while the number of required RF chains is significantly reduced.

Based on the spatially sparse hybrid precoding, several evolved hybrid precoding schemes have been proposed. In [11], a low-complexity version of the spatially sparse hybrid precoding is proposed. The main contributions of this work include: (1) derivation and integration of a matrix-inversion-bypass OMP algorithm to eliminate the matrix inversion operations; (2) development of a specific precoding reconstruction algorithm for the hardware implementation by considering the mm-Wave channel properties; and (3) design and implementation of a precoding reconstruction processor in an application-specific integrated circuit (ASIC) chip. In [12], the mm-Wave massive MIMO system with partial channel knowledge is considered, where the BS and the user only know their own local angles of arrival (AoAs). In such a scenario, [12] proposes a modified spatially sparse hybrid precoding accordingly to achieve the near-optimal performance. In [13], the spatially sparse hybrid precoding is combined with channel estimation, and a multi-resolution codebook is designed to estimate the AoA/AoD.

2.1 Deep Learning in Hybrid Precoding

As a class of machine learning techniques, Deep Learning (DL) has gained much interest recently for the solution of many challenging problems such as speech recognition, visual object recognition, and language processing [14, 15]. DL has several advantages such as low computational complexity when solving optimization-based or combinatorial search problems and the ability to extrapolate new features from a limited set of features contained in a training set [14]. Hybrid precoding matrices are designed using an explicit estimation of mm-Wave channel, which itself is a non-trivial task due to the involvement of massive MIMO with large antenna arrays at the transceivers, which imposes high training overhead and strict hardware constraints on RF chains.

The hybrid precoding has been developed to limit the power consumption and hardware cost of mm-Wave based systems, but the existing hybrid precoding methods have a high computational complexity. Deep learning can optimize the hybrid precoding in an mm-Wave system, following its remarkable performance when applied to massive MIMO based on the further decomposition of the baseband precoding matrix in hybrid precoding. The topology of the fully-connected phase shifter network in hybrid precoding structure is similar to neural networks. The authors in [2] considered the integration of DL into mm-Wave massive MIMO for the first time in literature and proposed a high-efficiency hybrid precoding scheme and concluded that the mm-Wave massive MIMO system can be optimized using deep learning. The DL method can fully extract the sparse features and leverage them to thoroughly learn the whole communication system; this branch of frameworks will be very appealing in next-generation communication networks.

2.1.1 Review of deep learning

The modern term "deep learning" that goes beyond the neuroscientific perspective inspired by the ML technique, is considered as a better principle of learning multiple levels of composition [16]. The simplest deep learning models is linear model, which is expressed as

$$f(\mathbf{v}, \mathbf{w}) = \sum_{i=1}^{n} v_i w_i, \tag{4}$$

where **w** represents the weight of the network, and this model is designed to take n input values as $\{v_1, v_2, ..., v_n\}$. Also, $f(\cdot)$ represents the output of the model, which can classify two different branches by identifying whether $f(\mathbf{v}, \mathbf{w})$ is positive or negative. Then, motivated by the basic idea of more computational units can facilitate intelligent interaction manners, many works develop new models that consist of multiple units.

Lately, a large breeds of deep learning architectures are based on a model neuron named the rectified linear unit. Another milestone of the deep learning was the successful use of back-propagation (BP) to train DNN with internal representations [17]. Inspired by this movement, the long short-term memory (LSTM) algorithm [18] was developed and it elevates the performance of the natural language processing (NLP). In recent decades, Geoffrey Hinton exhibited

that a kind of neural network called deep belief network can be optimized using a strategy named greedy layer-wise pretraining [19], and it brings a breakthrough in deep learning area among research community. Other research groups quickly showed that the same method can be adopted to train many other kinds of DNN [20] and systematically enhance generalization on test examples. Synchronously, some works have emphasized that DNN outperforms competing artificial intelligence (AI) systems based on other ML methods.

Organization *The rest of the report is organized as follows, In Section 3, the problems related to the hybrid precoding in mm-Wave massive MIMO systems are discussed, Section 4 and Section 5 discuss about two of the works [1] and [2] chosen to address the problems in hybrid precoding of mm-Wave massive MIMO systems. In Section 7, the critical analysis of these two works has been presented along with the potential future directions of research in this area. Finally, Section 8 concludes the report.*

Notations: *Vectors and matrices are represented by lower-case and upper-case boldface letters, respectively; transpose, conjugate transpose, inversion and determinant of a matrix are represented by* $(\cdot)^T$, $(\cdot)^H$, $(\cdot)^{-1}$ *and* $|\cdot|$, *respectively;* l_1*-norm,* l_2*-norm of a vector and Frobenius norm of a matrix are represented by* $\|\cdot\|_1$, $\|\cdot\|_2$ *and* $\|\cdot\|_F$, *respectively; Real and Imaginary part of a complex number are represented by Re*$\{\cdot\}$ *and Im*$\{\cdot\}$, *respectively; Expectation is represented by* $\mathbb{E}(\cdot)$ *and* $N \times N$ *identity matrix is represented by* $\boldsymbol{I}_N$.

3 Problem Statement

Hybrid analog and digital precoding techniques in mm-Wave massive MIMO systems have drawn significant attention of researchers for their capability of achieving high data rates and energy-efficient hardware implementation. However, the two major challenges in hybrid precoding desing that need to be addressed for mm-Wave massive MIMO systems are

1. High computational complexity
2. Poor system performance

In mm-Wave massive MIMO systems, the essence of hybrid precoding is to use two constrained matrices to approach the fully digital precoding matrix and accordingly, the intuitive solution of hybrid precoding is to decompose the fully digital precoding under given constraints.

As the constraints of analog matrix should be considered during decomposition, the computational complexity is very high. In the past few years, researchers have provided different methods for reducing the computational complexity or improving the precoding performance. However, the hybrid precoding performances have been compromised in the low-complexity solutions of these conventional methods. These conventional methods also bring great challenges in addressing the non-convex constant modulus constraints on the analog precoder imposed by the use of phase shifters (PSs) and fail to exploit the structural characteristics of the mm-Wave signals. Therefore, it is extremely important to introduce new methods for enhancing the performance and reducing the complexity issues in hybrid precoding schemes for the mm-Wave massive MIMO systems. In this report, the considered two papers [1, 2] address these issues and avoid the use of conventional methods in providing low-complexity solutions.

4 Hybrid Precoding in Millimeter-Wave Massive MIMO System

4.1 Problem Formulation

In the work [1], authors have considered the sub-connected architecture for hybrid precoding in mm-Wave MIMO systems with NM base station (BS) antennas and N RF chains where each RF chain is associated to M phase shifters (PSs) and each of these M PSs are further connected to a sub-antenna array with only M antennas which is a subset of the total BS antennas. The BS transmits N independent data streams to users with K receive antennas and these N data streams in the baseband are precoded by a digital precoder $\mathbf{D}$ where $\mathbf{D} = [d_1, d_2, \ldots, d_N]$, is a diagonal matrix and $d_n \in \mathbb{R}$ for $n = 1, 2, \ldots, N$. The digitally precoded signal passes through corresponding RF chain and reaches to M PSs associated to each RF chain to perform analog precoding. This can be represented by the analog weighting vector $\bar{\mathbf{a}}_n = \mathbb{C}^{M\times 1}$, elements of which is of same magnitude $1/\sqrt{M}$ but different phases. After the analog precoding, each data stream is finally transmitted by the corresponding sub-antenna array associated to each RF chain and the received signal vector $\mathbf{y} = [y_1, y_2, \ldots, y_k]^T$ at the user in a narrowband system is given as

$$\mathbf{y} = \sqrt{\rho}\mathbf{HADs} + \mathbf{n} = \sqrt{\rho}\mathbf{HPs} + \mathbf{n}, \tag{5}$$

where ρ represents the average received power; $\mathbf{H} \in \mathbb{C}^{K\times NM}$ represents the channel matrix, $\mathbf{A}$ represents the $NM \times N$ analog precoding matrix which comprises N analog weighting vectors $\{\bar{\mathbf{a}}_m\}_{m=1}^{N}$ given as

$$\begin{bmatrix} \bar{\mathbf{a}}_1 & \mathbf{0} & \ldots & \mathbf{0} \\ \mathbf{0} & \bar{\mathbf{a}}_2 & & \mathbf{0} \\ \vdots & & \ddots & \vdots \\ \mathbf{0} & \mathbf{0} & \ldots & \bar{\mathbf{a}}_N \end{bmatrix}_{NM\times N}, \tag{6}$$

$\mathbf{s} = [s_1, s_2, \ldots, s_N]^T$ is the transmitted signal vector in the baseband. In this work, the widely used Gaussian signals with normalized signal power $\mathbb{E}(\mathbf{ss}^H) = \frac{1}{N}\mathbf{I}_N$ is used. The hybrid precoding matrix of size $NM \times N$ is represented by $\mathbf{P} = \mathbf{AD}$ and satisfies $\|\mathbf{P}\|_F \leq N$ to achieve the total transmit power constraint. Lastly, $\mathbf{n} = [n_1, n_2, \ldots, n_N]^T$ is an independent and identically

distributed (i.i.d.) additive white Gaussian noise (AWGN) $\mathcal{CN}(0, \sigma^2)$ vector.

In this work, the aim is to maximize the total achievable rate R of mm-Wave MIMO systems where R is given as

$$R = \log_2\big(|\mathbf{I}_K + \frac{\rho}{N\sigma^2}\mathbf{HPP}^H\mathbf{H}^H|\big). \tag{7}$$

As seen in (5), $\mathbf{P}$ can be represented as $\mathbf{P} = \mathbf{AD}$ where both $\mathbf{A}$ and $\mathbf{D}$ are the diagonal matrices, the design of $\mathbf{P}$ is depends on three constraints which are given as:

1. *Constraints 1:* $\mathbf{P}$ should be a block diagonal matrix similar to A as shown in (6). This represents $\mathbf{P} = \text{diag}\{\bar{\mathbf{p}}_1, \ldots, \bar{\mathbf{p}}_N\}$, where $\bar{\mathbf{p}_n} = d_n\bar{\mathbf{a}_n}$ is the $M \times 1$ non-zero vector of the n-th column $\mathbf{p}_n$ of P, i.e., $p_n = [\mathbf{0}_{1\times M(n-1)},\ \bar{\mathbf{p}_n},\ \mathbf{0}_{1\times M(N-n)}]^T$.

2. *Constraint 2:* The non-zero elements of each column of $\mathbf{P}$ should have the same amplitude since the digital precoding matrix $\mathbf{D}$ is a diagonal matrix, and the amplitude of non-zero elements of the analog precoding matrix $\mathbf{A}$ is fixed to $1/\sqrt{M}$.

3. *Constraint 3:* The Frobenius norm of $\mathbf{P}$ should satisfy $\|\mathbf{P}\|_F \leq N$ to meet the total transmit power constraint, where N is number of transmitted data stream which is equal to the number of RF chains.

These constraints on $\mathbf{P}$ are non-convex and so, the solution for the minimization of the total achievable rate in (7) is intractable. The diagonal structure of hybrid precoding matrix $\mathbf{P}$ suggests that the precoding of different sub-antenna arrays are independent, so the total achievable rate (7) is decomposed into a series of sub-rate optimization problems for each sub-antenna array individually.

The hybrid precoding matrix $\mathbf{P}$ is divided as $\mathbf{P} = [\mathbf{P}_{N-1}\mathbf{p}_N]$, with $\mathbf{p}_N$ be the N-th column of $\mathbf{P}$ and $\mathbf{P}_{N-1}$ be a $NM \times (N-1)$ matrix which contains first $N-1$ columns of $\mathbf{P}$. Then, the total

achievable rate R in (7) is rewritten as

$$\begin{aligned}
R &= \log_2\Big(\Big|\mathbf{I}_K + \frac{\rho}{N\sigma^2}\mathbf{H}\mathbf{P}\mathbf{P}^H\mathbf{H}^H\Big|\Big) \\
&= \log_2\Big(\Big|\mathbf{I}_K + \frac{\rho}{N\sigma^2}\mathbf{H}[\mathbf{P}_{N-1}\mathbf{p}_N][\mathbf{P}_{N-1}\mathbf{p}_N]^H\mathbf{H}^H\Big|\Big) \\
&= \log_2\Big(\Big|\mathbf{I}_K + \frac{\rho}{N\sigma^2}\mathbf{H}\mathbf{P}_{N-1}\mathbf{P}_{N-1}^H\mathbf{H}^H + \frac{\rho}{N\sigma^2}\mathbf{H}\mathbf{p}_N\mathbf{p}_N^H\mathbf{H}^H\Big|\Big) \\
&\overset{(a)}{=} \log_2(|\mathbf{T}_{N-1}|) + \log_2\Big(\Big|\mathbf{I}_K + \frac{\rho}{N\sigma^2}\mathbf{T}_{N-1}^{-1}\mathbf{H}\mathbf{p}_N\mathbf{p}_N^H\mathbf{H}^H\Big|\Big) \\
&\overset{(b)}{=} \log_2(|\mathbf{T}_{N-1}|) + \log_2\Big(\Big|1 + \frac{\rho}{N\sigma^2}\mathbf{p}_N^H\mathbf{H}^H\mathbf{T}_{N-1}^{-1}\mathbf{H}\mathbf{p}_N\Big|\Big),
\end{aligned} \tag{8}$$

The second term $\log_2\Big(\Big|1 + \frac{\rho}{N\sigma^2}\mathbf{p}_N^H\mathbf{H}^H\mathbf{T}_{N-1}^{-1}\mathbf{H}\mathbf{p}_N\Big|\Big)$ in (8) is the achievable sub-rate of the the N-th sub-antenna array, while the first term $\log_2(|\mathbf{T}_{N-1}|)$ shares the same form as (7). This implication helps in further decomposition of $\log_2(|\mathbf{T}_{N-1}|)$ as

$$\log_2(|\mathbf{T}_{N-2}|) + \log_2\Big(\Big|1 + \frac{\rho}{N\sigma^2}\mathbf{p}_{N-1}^H\mathbf{H}^H\mathbf{T}_{N-2}^{-1}\mathbf{H}\mathbf{p}_{N-1}\Big|\Big).$$

After N such decompositions, the total achievable rate R in (7) is given as

$$R = \sum_{n=1}^{N}\log_2\Big(1 + \frac{\rho}{N\sigma^2}\mathbf{p}_n^H\mathbf{H}^H\mathbf{T}_{n-1}^{-1}\mathbf{H}\mathbf{p}_n\Big), \tag{9}$$

where $\mathbf{T}_n = \mathbf{I}_K + \frac{\rho}{N\sigma^2}\mathbf{H}\mathbf{P}_n\mathbf{P}_n^H\mathbf{H}^H$ and $\mathbf{T}_0 = \mathbf{I}_N$. These series of sub-rate optimization problems of sub-antenna arrays can be optimized one by one. The use of SIC for multiuser detection enables to optimize the achievable sub-rate of each sub-antenna array and update the corresponding matrix $\mathbf{T}$, successively. Fig. 4 [1] shows the diagram of the proposed SIC-based hybrid precoding.

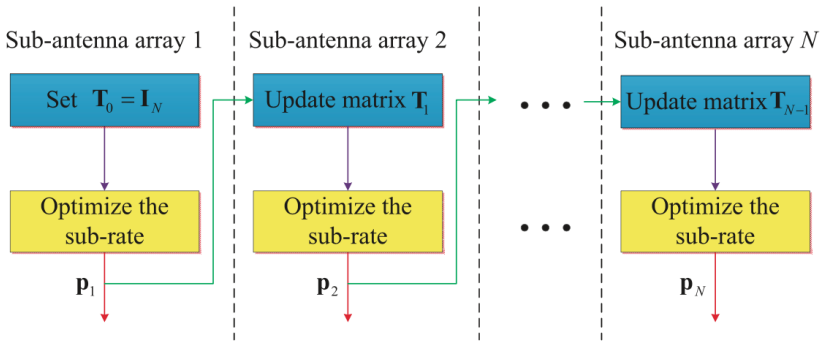

Figure 4: Proposed SIC-based hybrid precoding

4.2 Solution Methodology

4.2.1 Solution to the subrate optimization problem

According to (9), the sub-rate optimization problem of the n-th sub-antenna array by designing the n-th precoding vector $\mathbf{p}_n$ is given as

$$\mathbf{p}_n^{\text{opt}} = \arg\max_{\mathbf{p}_n \in \mathcal{F}} \log_2\left(1 + \frac{\rho}{N\sigma^2}\mathbf{p}_n^H \mathbf{G}_{n-1}\mathbf{p}_n\right), \tag{10}$$

where $G_{n-1} = \mathbf{H}^H\mathbf{T}_{n-1}^{-1}\mathbf{H}$, $\mathcal{F}$ is the set of all feasible vectors which satisfy the three constraints in Section 4.2. The n-th precoding vector $\mathbf{p}_n$ only has M non-zero elements from the $(M(n-1)+1)$-th one to the (Mn)-th one. Therefore, the sub-rate optimization problem in (10) can be written as

$$\bar{\mathbf{p}}_n^{\text{opt}} = \arg\max_{\bar{\mathbf{p}}_n \in \bar{\mathcal{F}}} \log_2\left(1 + \frac{\rho}{N\sigma^2}\bar{\mathbf{p}}_n^H \bar{\mathbf{G}}_{n-1}\bar{\mathbf{p}}_n\right), \tag{11}$$

where $\bar{\mathcal{F}}$ contains all possible $M \times 1$ vectors satisfying *Constraint 2* and *Constraint 3*, $\bar{\mathbf{G}}_{n-1}$ of size $M \times M$ is the corresponding sub-matrix of $\mathbf{G}_{n-1}$ which consists of the rows and columns of $\mathbf{G}_{n-1}$ from the $(M(n-1)+1)$-th one to the the (Mn)-th on, which is given as

$$\bar{\mathbf{G}}_{n-1} = \mathbf{R}\mathbf{G}_{n-1}\mathbf{R}^H = \mathbf{R}\mathbf{H}^H\mathbf{T}_{n-1}^{-1}\mathbf{H}\mathbf{R}^H, \tag{12}$$

where $\mathbf{R} = [\mathbf{0}_{M\times M(n-1)}\ \mathbf{I}_M\ \mathbf{0}_{M\times M(N-n)}]$ is the corresponding selection matrix.

The singular value decomposition (SVD) of the Hermitian matrix $\bar{\mathbf{G}}_{n-1}$ is defined as $\bar{\mathbf{G}}_{n-1} = \mathbf{V}\mathbf{\Sigma}\mathbf{V}^H$, where $\mathbf{\Sigma}$ is an $M \times M$ diagonal matrix which contains the singular values of $\bar{\mathbf{G}}_{n-1}$ in

a decreasing order and $\mathbf{V}$ is an $M \times M$ unitary matrix. The optimal unconstrained precoding vector of (11) is the first column $\mathbf{v}_1$ of $\mathbf{V}$, i.e., the first right singular vector of $\bar{\mathbf{G}}_{n-1}$ [3]. However, according to the contraints mentioned in Section 4.2, $\bar{\mathbf{p}}_n^{\text{opt}}$ cannot be chosen directly as v_1 since the elements of $\mathbf{v}_1$ do not obey the constraint of same amplitude (i.e. Constraint 2). To find a feasible solution to the sub-rate optimization problem (11), it is necessary to convert (11) into another equivalent form which is given by the following proposition:

Proposition 1: The optimization problem (11)

$$\bar{\mathbf{p}}_n^{\text{opt}} = \underset{\bar{\mathbf{p}}_n \in \bar{\mathcal{F}}}{\arg\max} \log_2\Big(1 + \frac{\rho}{N\sigma^2}\bar{\mathbf{p}}_n^H \bar{\mathbf{G}}_{n-1}\bar{\mathbf{p}}_n\Big)$$

is equivalent to the following optimization problem

$$\bar{\mathbf{p}}_n^{\text{opt}} = \underset{\bar{\mathbf{p}}_n \in \bar{\mathcal{F}}}{\arg\min} \|\mathbf{v}_1 - \bar{\mathbf{p}}_n\|_2^2, \tag{13}$$

where $\mathbf{v}_1$ is the first right singular vector of $\bar{\mathbf{G}}_{n-1}$.

Proposition 1 indicates that it is possible to find a feasible precoding vector $\bar{\mathbf{p}}_n$, which is sufficiently close to the optimal $\mathbf{v}_1$ but unpractical precoding vector v_1, to maximize the achievable sub-rate of the n-th sub-antenna array. Since $\bar{\mathbf{p}}_n = d_n\bar{\mathbf{a}}_n$ according to (5), the target $\|\mathbf{v}_1 - \bar{\mathbf{p}}_n\|_2^2$ in (13) is written as

$$\begin{aligned}
\|\mathbf{v}_1 - \bar{\mathbf{p}}_n\|_2^2 = & \\
&= (\mathbf{v}_1 - d_n\bar{\mathbf{a}}_n)^H(x\mathbf{v}_1 - d_n\bar{\mathbf{a}}_n) \\
&= \mathbf{v}_1^H\mathbf{v}_1 + d_n^2\bar{\mathbf{a}}_n^H\bar{\mathbf{a}}_n - 2d_n\text{Re}(\mathbf{v}_1^H\bar{\mathbf{a}}_n) \\
&\overset{(a)}{=} 1 + d_n^2 - 2d_n\text{Re}\big(\mathbf{v}_1^H\bar{\mathbf{a}}_n\big) \\
&= \Big(d_n - \text{Re}\big(\mathbf{v}_1^H\bar{\mathbf{a}}_n\big)\Big)^2 + \Big(1 - \big[\text{Re}\big(\mathbf{v}_1^H\bar{\mathbf{a}}_n\big)\big]^2\Big),
\end{aligned} \tag{14}$$

where (a) is obtained considering the facts that both $\bar{\mathbf{a}}$ and $\mathbf{v}_1$ have a fixed power of one, i.e., $\mathbf{v}_1^H\mathbf{v}_1 = 1$ and $\bar{\mathbf{a}}_n^H\bar{\mathbf{a}_n} = 1$, since $\mathbf{v}_1$ is the first column of the unitary matrix $\mathbf{V}$ and each element of $\bar{\mathbf{a}}_n$ has the same amplitude $1/\sqrt{M}$. From (14), it can be seen that the distance between $\bar{\mathbf{p}}_n$ and $\mathbf{v}_1$ consists of two parts. The first one is $(d_n - \text{Re}(\mathbf{v}_1^H\bar{\mathbf{a}}_n))^2$, which can be minimized to zero

by chosing $d_n = \text{Re}(\mathbf{v}_1^H \bar{\mathbf{a}}_n)$. The second one is $(1 - [\text{Re}(\mathbf{v}_1^H \bar{\mathbf{a}}_n)]^2)$, which can be minimized by maximizing $|\text{Re}(\mathbf{v}_1^H \bar{\mathbf{a}}_n)|$. As $\mathbf{v}_1^H \mathbf{v}_1 = 1$ and $\bar{\mathbf{a}}_n^H \bar{\mathbf{a}}_n = 1$, the optimal $\bar{\mathbf{a}}_n^{\text{opt}}$ to maximize $|\text{Re}(\mathbf{v}_1^H \bar{\mathbf{a}}_n)|$ is

$$\bar{\mathbf{a}}_n^{\text{opt}} = \frac{1}{\sqrt{M}} e^{j\text{angle}(\mathbf{v}_1)}, \tag{15}$$

where $\text{angle}(\mathbf{v}_1)$ represents the phase vector of $\mathbf{v}_1$ i.e., each element of $\bar{\mathbf{a}}_n^{\text{opt}}$ shares the same phase as the corresponding element of $\mathbf{v}_1$. Correspondingly, the optimal choice of d_n^{opt} is

$$d_n^{\text{opt}} = \text{Re}\Big(\mathbf{v}_1^H \bar{\mathbf{a}}_n\Big) = \frac{1}{\sqrt{M}} \text{Re}\Big(\mathbf{v}_1^H e^{j\text{angle}(\mathbf{v}_1)}\Big) = \frac{\|\mathbf{v}_1\|_1}{\sqrt{M}}. \tag{16}$$

Based on (15) and (16), th optimal solution $\bar{\mathbf{p}}_n^{\text{opt}}$ to te optimization problem (13) can be obtained by

$$\bar{\mathbf{p}}_n^{\text{opt}} = d_n^{\text{opt}} \bar{\mathbf{a}}_n^{\text{opt}} = \frac{1}{M} \|\mathbf{v}_1\|_1 \, e^{j\text{angle}(\mathbf{v}_1)}. \tag{17}$$

As $\mathbf{v}_1$ is the first column of the unitary matrix $\mathbf{V}$, each element v_i of $\mathbf{v}_1$ (for $i = 1, \ldots, M$) has the amplitude less than one. Therefore, $\|\bar{\mathbf{p}}_n^{\text{opt}}\|_2^2 \leq 1$. The optimal solution $\bar{\mathbf{p}}_n^{\text{opt}}$ for $n = 1, 2, \ldots, N$ have a similar form. So, it can be concluded that

$$\left\|\mathbf{P}^{\text{opt}}\right\|_F^2 = \left\| \text{diag}\Big\{ \bar{\mathbf{p}}_1^{\text{opt}}, \ldots, \bar{\mathbf{p}}_N^{\text{opt}} \Big\} \right\|_F^2 \leq N, \tag{18}$$

which satisfies the total transmit power constraint (*Constraint 3*).

Now, when the $\mathbf{P}^{\text{opt}}$ is obtained for the n-th sub-antenna array, the matrices $\mathbf{T}_n = \mathbf{I}_K + \frac{\rho}{N\sigma^2} \mathbf{H} \mathbf{P}_n \mathbf{P}_n^H \mathbf{H}^H$ (9) and $\bar{\mathbf{G}}_{n-1} = \mathbf{R}\mathbf{H}^H \mathbf{T}_{n-1}^{-1} \mathbf{H}\mathbf{R}^H$ (12) can be updated. Then, the same method can be applied again to optimize the achievable sub-rate of the $(n+1)$-th sub-antenna array. The steps for solving the sub-rate optimization problem of the n-th sub-antenna array are summarized as follows:

Step 1: Execute the SVD of $\bar{\mathbf{G}}_{n-1}$ to obtain $\mathbf{v}_1$;

Step 2: Let $\bar{\mathbf{p}}_n = \frac{1}{M} \|\mathbf{v}_1\|_1 \, e^{j\text{angle}(\mathbf{v}_1)}$ as the optimal solution to the current n-th sub-antenna array;

Step 3: Update matrices $\mathbf{T}_n = \mathbf{I}_K + \frac{\rho}{N\sigma^2} \mathbf{H} \mathbf{P}_n \mathbf{P}_n^H \mathbf{H}^H$ and $\bar{\mathbf{G}}_{n-1} = \mathbf{R}\mathbf{H}^H \mathbf{T}_{n-1}^{-1} \mathbf{H}\mathbf{R}^H$ for the next $(n+1)$-th sub-antenna array.

The optimal solution $\bar{\mathbf{p}}_n$ is obtained with the above-mentioned method, but the computation of SVD of $\bar{\mathbf{G}}_{n-1}$ (*Step 1*) and the matrix $\bar{\mathbf{G}}_n$ (*Step 3*) which involve the matrix inversion of large size, leads to high computational complexity and high energy consumption. In the next Section 4.2.2, a low-complexity algorithm is proposed to obtain $\bar{\mathbf{p}}_n^{\text{opt}}$ without the complicated SVD and matrix inversion.

4.2.2 Low-complexity algorithm to obtain the optimal solution

It can be seen from *Step 1* mentioned in Section 4.2.1 that the SVD of $\bar{\mathbf{G}}_{n-1}$ need not to be computed to achieve $\mathbf{\Sigma}$ and $\mathbf{V}$, since the first column $\mathbf{v}_1$ of $\mathbf{V}$ is sufficient to obtain $\bar{\mathbf{p}}_n^{\text{opt}}$. Based on this observation, the simple power iteration algorithm [21], which is used to compute the largest eigenvalue and the corresponding eigenvector of a diagonalizable matrix is exploited. Since, $\bar{\mathbf{G}}_{n-1}$ is a Hermitian matrix, the following can be written:

(1) $\bar{\mathbf{G}}_{n-1}$ is also a diagonalizable matrix;

(2) The singular value (right singular vectors) of $\bar{\mathbf{G}}_{n-1}$ are the same as the eigenvalues (eigenvectors).

This indicates that the power iteration algorithm can also be utilized to compute $\mathbf{v}_1$ and the largest singular value Σ_1 of $\bar{\mathbf{G}}_{n-1}$ with low complexity. The pseudo-code in **Algorithm 1** shows that the power iteration algorithm initialized with $\mathbf{u}^{(0)} \in \mathbb{C}^{M\times 1}$, and in each iteration (s), the auxiliary vector $\mathbf{z}^{(s)} = \bar{\mathbf{G}}_{n-1}\mathbf{u}^{(s-1)}$ is computed first. After this, the element of $\mathbf{z}^{(s)}$, which is having the largest amplitude, represented by $m^{(S)}$, is extracted. The power iteration algorithm will continue until the number of iterations reaches the predefined number S. The output $m^{(S)}$ and $\mathbf{u}^{(S)}/\left\|\mathbf{u}^{(S)}\right\|_2$ are the largest singular value Σ_1 and the first right singular vector $\mathbf{v}_1$ of $\bar{\mathbf{G}}_{n-1}$, respectively. It can be seen that [21]

$$m^{(s)} = \Sigma_1\Big[1 + \mathcal{O}\Big(\Big(\frac{\Sigma_2}{\Sigma_1}\Big)^s\Big)\Big], \tag{19}$$

where Σ_2 represents the second largest singular value of $\bar{\mathbf{G}}_{n-1}$. Using (19), it can be concluded that $m^{(s)}$ converges to Σ_1 and $\mathbf{u}^{(s)}/\left\|\mathbf{u}^{(s)}\right\|_2$ converges to $\mathbf{v}_1$ as long as $\Sigma_1 \neq \Sigma_2$, which are written

as

$$\lim_{s\to\infty} m^{(s)} = \Sigma_1, \quad \lim_{s\to\infty} \frac{\mathbf{u}^{(s)}}{\left\|\mathbf{u}^{(s)}\right\|_2} = \mathbf{v}_1. \tag{20}$$

To further increase the convergence rate of the power iteration algorithm, the Aitken acceleration method [22] is utilized. It helps to calculate

$$\begin{cases} n^{(s)} = m^{(s)}, \quad \text{for} \quad 1 \leq s \leq 2, \\ n^{(s)} = \frac{m^{(s)}m^{(s-2)} - (m^{(s-1)})^2}{m^{(s)} - 2m^{(s-1)} + m^{(s-2)}} \quad \text{for} \quad 2 \leq s \leq S. \end{cases} \tag{21}$$

Then, $\mathbf{u}^{(s)}$ and Σ_1 will be changed to $\mathbf{u}^{(s)} = \frac{\mathbf{z}^{(s)}}{n^{(s)}}$ and $\Sigma_1 = n^{(S)}$, respectively.

Proposition 2: The complexity of the matrices $\bar{\mathbf{G}}_n = \mathbf{R}\mathbf{H}^H\mathbf{T}_n^{-1}\mathbf{H}\mathbf{R}^H$ and $\mathbf{T}_n = \mathbf{I}_K + \frac{\rho}{N\sigma^2}\mathbf{H}\mathbf{P}_n\mathbf{P}_n^H\mathbf{H}^H$ can be reduced by the following simplification

$$\bar{\mathbf{G}_n} \approx \bar{\mathbf{G}}_{n-1} - \frac{\frac{\rho}{N\sigma^2}\Sigma_1^2\mathbf{v}_1\mathbf{v}_1^H}{1 + \frac{\rho}{N\sigma^2}\Sigma_1}, \tag{22}$$

where Σ_1 and $\mathbf{v}_1$ are the largest singular value and first right singular vector of $\bar{\mathbf{G}_n}$, respectively. According to ***Proposition 2***, Σ_1 and $\mathbf{v}_1$ obtained by **Algorithm 1** can be exploited to update $\bar{\mathbf{G}_n}$, where instead of complex matix-to-matrix multiplication and matrix inversion, only one vector-to-vector multiplication is involved.

The pseudo-code of the proposed SIC-based hybrid precoding is summarized in **Algorithm 2**. Initially, based on **Algorithm 1**, the largest singular value Σ_1 and the right singular vector $\mathbf{v}_1$ of $\bar{\mathbf{G}}_{n-1}$ is calculated. Then, the optimal precoding vector of the n-th sub-antenna array (Section 4.2.1) is obtained by utilizing $\mathbf{v}_1$. In the end, based on ***Proposition 2***, $\bar{\mathbf{G}}_n$ is updated with low-complexity for the next iteration. This process is continued until it reaches to the final N-th sub-antenna array. When N iterations are executed, the optimal digital, analog and hybrid precoding matrices **D**, **A** and **P** are obtained, respectively.

4.3 Numerical Results

In this section, simulation results for the achievable rate and energy efficiency to evaluate the performance of the proposed SIC-based hybrid precoding have been provided and the perfor-

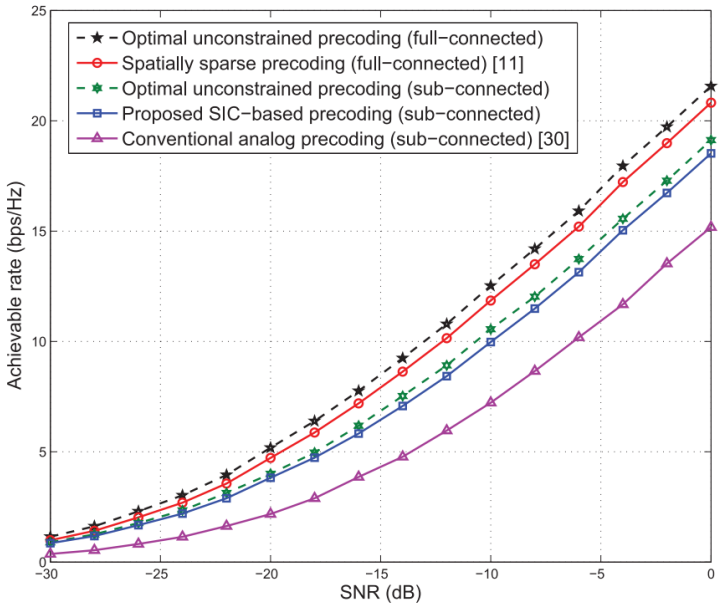

Figure 5: Achievable rate comparison for an $NM \times K = 64 \times 16$ ($N = 8$) mm-Wave MIMO system.

mance is compared to the fully-connected architecture of spatially sparse precoding [3] and the optimal unconstrained precoding based on the SVD of the channel matrix. The sub-connected architecture of conventional analog precoding [23] and the optimal unconstrained precoding (i.e., $\bar{\mathbf{p}}_n^{\text{opt}} = \mathbf{v}_1$) is also considered as benchmarks for comparision.

For simulation purpose, the parameters are chosen as follows. The channel matrix has been generated based on the channel model [13] described in Section 4.1. The number of effective channel paths is $L = 3$ [3]. The carrier frequency is set as 28 GHz [24]. Both the transmit and receive antenna arrays are ULAs with antenna spacing $d = \lambda/2$. The AoDs are assumed to follow the uniform distribution within $\left[-\frac{\pi}{6}, \frac{\pi}{6}\right]$ [25]. The AoAs are assumed to follow the uniform distribution within $\left[-\pi, \pi\right]$. The maximum number of iterations is set as $S = 5$ to run the **Algorithm 2**. Lastly, SNR is defined as $\frac{\rho}{\sigma^2}$.

Initially, the channel state information (CSI) is considered as perfect. Fig. 5 shows the achievable rate comparison in mm-Wave MIMO system, where $NM \times K = 64 \times 16$ and the number of RF chains is $N = 8$. from Fig. 5 [1], it can be observed that the proposed SIC-based hybrid precoding is superior to the conventional analog precoding with sub-connected architecture in the whole simulated SNR range. Also, the near optimal performance of SIC-based hybrid precoding is verified as it reaches around 99% of the rate achieved by the optimal

unconstrained precoding with sub-connected architecture. More importantly, Fig. 5 shows that the performance of SIC-based hybrid precoding is close to the spatially sparse precoding and the optimal unconstrained precoding with fully connected architecture.

Next, the energy efficiency η of the SIC-based hybrid precoding is evaluated as

$$\eta = \frac{R}{P_{\text{total}}} = \frac{R}{P_{\text{t}} + N_{\text{RF}} P_{\text{RF}} + N_{\text{PS}} P_{\text{PS}}} (\text{bps/Hz/W}), \tag{23}$$

where $P_{\text{total}} \triangleq P_{\text{t}} + N_{\text{RF}} P_{\text{RF}} + N_{\text{PS}} P_{\text{PS}}$ is the total energy con- sumption, P_{t} is the transmitted energy, P_{RF} is the energy consumed by RF chain, P_{PS} is the energy consumed by PS, N_{RF} and N_{PS} are the numbers of required RF chains and PSs, respectively. The practical values of these parameters are taken as $P_{\text{RF}} = 250$ mW, $P_{\text{PS}} = 1$ mW, and $P_{\text{t}} = 1$ W in a small cell transmission scenario, since mm-Wave is more likely to be applied in small cells. Fig. 6 shows the energy efficiency comparison against the number of RF chains N, where SNR $= 0$ dB, $NM = K = 64$. Both the conventional spatially sparse precoding and the proposed SIC-based precoding can achieve higher energy efficiency than the optimal unconstrained precoding (also known as the fully digital precoding), especially when the number of RF chains N is limited. Besides, the proposed SIC- based precoding is more energy efficient than the conventional spatially sparse precoding.

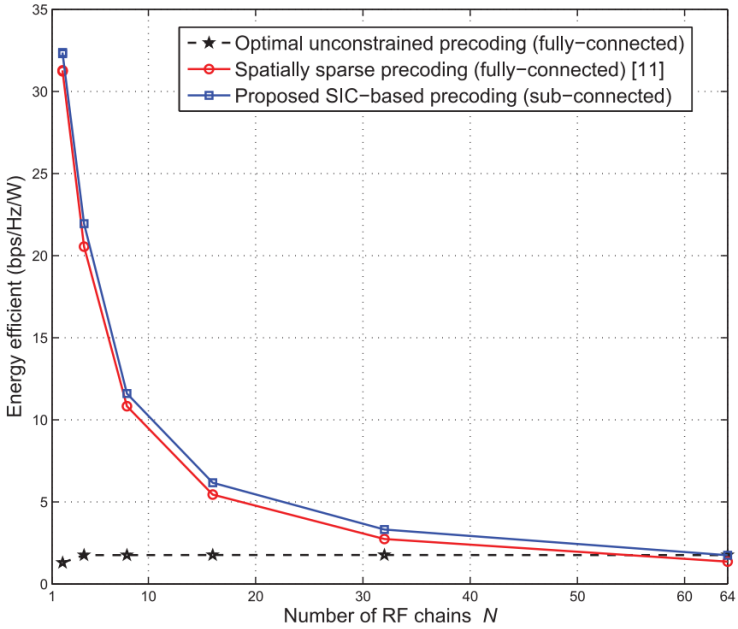

Figure 6: Energy efficiency comparison against the numbers of RF chains N, where $NM = K = 64$.

5 Hybrid Precoding in Deep Learning based Millimeter-Wave Massive MIMO System

5.1 Problem Formulation

In [2], a typical mm-Wave massive MIMO system is considered where a BS is designed with an uniform linear array (ULA) of N_t transmit antennas and user with N_r receive antennas. The BS sends N_s independent data streams to the user assuming that there are no information available on any of the communication link. It is also assumed that the BS and the user have N_t^{RF} and N_r^{RF} RF chains, respectively, which meet the $N_s \leq N_t^{RF} \leq N_t$ and $N_t \leq N_r^{RF} \leq N_r$ requirements [3]. The authors have used Saleh-Valenzuela (SV) channel model where the channel matrix $\mathbf{H}$. A high-dimensional analog precoder and a low-dimensional digital precoder is assumed as $\mathbf{D}_A \in \mathbb{C}^{N_t \times N_t^{RF}}$ and $\mathbf{D}_D \in \mathbb{C}^{N_t^{RF} \times N_s}$, respectively. A hybrid precoder is the combination of these two precoders and is represented as $\mathbf{D} = \mathbf{D}_A\mathbf{D}_D \in \mathbb{C}^{N_t \times N_s}$. Hence, the transmitted signal x is given as

$$x = \mathbf{D}\mathbf{s} = \mathbf{D}_A\mathbf{D}_D\mathbf{s}, \tag{24}$$

where $\mathbf{s} \in \mathbb{C}^{N_s \times 1}$ represents the source signal with normalized power $E[\mathbf{s}\mathbf{s}^H] = \mathbf{I}_{N_s}$ and to satisfy the constraint of transmit power, it is assumed that $\text{tr}\{\mathbf{D}\mathbf{D}^H\} \leq N_s$ [26]. The received signal vector is given as

$$\begin{aligned} \mathbf{y} &= \mathbf{B}^H\mathbf{H}\mathbf{x} + \mathbf{B}^H\mathbf{n} \\ &= (\mathbf{B}_D^H\mathbf{B}_A^H)\mathbf{H}\mathbf{D}_A\mathbf{D}_D\mathbf{s} + \mathbf{B}_D^H\mathbf{B}_A^H\mathbf{n}, \end{aligned} \tag{25}$$

where $n \sim \mathcal{CN}(0, \sigma^2\mathbf{I}_{N_s})$ represents the AWGN noise. $\mathbf{B}_D \in \mathbb{C}^{N_r^{RF} \times N_s}$ and $\mathbf{B}_A \in \mathbb{C}^{N_r \times N_r^{RF}}$ represent a digital combiner and a analog combiner, respectively and $\mathbf{B}^H = \mathbf{B}_D^H\mathbf{B}_A^H$ represents a hybrid combiner. The analog precoder is always installed using phase shifters (PSs) and elements of $\mathbf{D}_A$ and $\mathbf{B}_A$ need to meet the requirements given as

$$|\{\mathbf{D}_A\}_{i,j}| = \frac{1}{\sqrt{N_t}}, \;\; |\{\mathbf{B}_A\}_{i,j}| = \frac{1}{\sqrt{N_r}}. \tag{26}$$

To improve the performance of the hybrid precoding in mm-Wave massive MIMO system, it is important to exploit the sparsity present in the mm-Wave channel and so, a deep neural network (DNN) is employed to construct a novel precoding framework.

5.2 Solution Methodology

5.2.1 DNN Learning Framework

In the deep learning area, DNN is considered as one of the most popular generative models. According to the well- known *universal approximation theorem* [27], it is noted that a feed-forward network with a single hidden layer processed by multilayer perception mechanism can approximate continuous functions on compact subsets of R^n . As a multilayer processor, the DNN is capable of dealing with many non-convex and non-linear issues. Based on the massive MIMO system, high computation complexity is a key limit in terms of channel estimation and DOA estimation. Through non-linear operation and propagation, this problem can be settled with the DNN. Also, the multilayer perception mechanism and special training policy promote the DNN to be a commendable tool to leverage the sparsity characteristics of the massive MIMO. Here, let us introduce the DNN briefly. DNN, which can be regarded as a deeper version ofartificial neural

networks (ANN), is designed as a neural network with many hidden layers. In par- ticular, there are multiple neurons implementing in each hidden layer, as well as an output with weighted sum of these neurons operated by a nonlinear function. In order to realize recognition and representation operation, the DNN is processed by activation. In general, the Sigmoid $\sigma(\cdot)$ function and the ReLU$(\cdot)$ function are the most universal choices in the nonlinear operation, given as

$$\sigma(a) = \frac{1}{1+e^{-\alpha}}, \ \ \text{ReLU}(a) = \max(0, a) \tag{27}$$

where a is denoted as the argument of the function. The mapping between the input $\mathbf{v}$ and the output $\mathbf{o}$ of the DNN of the massive MIMO system is obtained as

$$\mathbf{o} = f(\mathbf{v}, w) = f^{(n-1)}(f^{(n-2)}(\cdots f^{1}(\mathbf{v}))), \tag{28}$$

where n and w represent the number of layers in the neural network and the weights of the neural network, respectively.

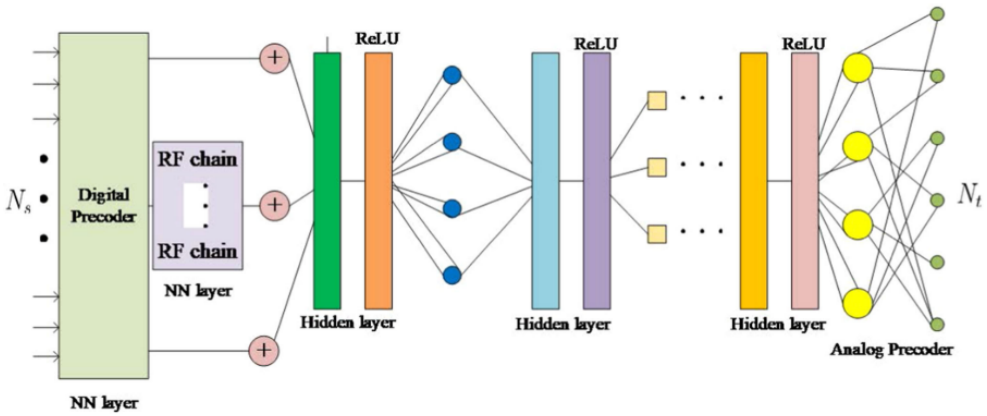

Figure 7: Deep learning-based mm-Wave hybrid precoding framework.

Fig. 7 [2] shows the constructed DNN framework to realize hybrid precoding. The input layer is a fully-connected (FC) layer with 128 neurons for capturing features of the input data. In this layer, the length of each training sequence is determined by its dimension. The next two hidden layers are also FC layers with 400 neurons and 256 neurons, respectively and used for processing encoding operation. A 200 neurons AWGN noise layer is also considered for mixing distortion. Subsequently, the next two hidden layers with 128 neurons and 64 neurons, respectively, are

considered for decoding. The output layer is deployed to generate expected output signals of the network. The ReLU function is used as the activation function of the input layer and the hidden layers. To enforce the power constraint in the output layer, a special activation function is designed as

$$f(s) = \min(\max(\mathbf{s}, 0), N_s). \tag{29}$$

5.2.2 Learning policy

To simplify the mapping relation of the hybrid precoding, GMD method is employed to decompose the complex mm-Wave massive MIMO channel matrix and $\mathbf{H}$ is formulated by

$$\mathbf{y} = \mathbf{WQR}^H = [\mathbf{W}_1, \mathbf{W}_2] \begin{bmatrix} \mathbf{Q}_1 & * \\ \mathbf{0} & \mathbf{Q}_2 \end{bmatrix} \begin{bmatrix} \mathbf{R}_1^H \\ \mathbf{R}_2^H \end{bmatrix}, \tag{30}$$

where the combiner $\mathbf{W}_1 \in \mathbb{C}^{N_r \times N_s}$ and $\mathbf{R}_1 \in \mathbb{C}^{N_t \times N_s}$ is the precoder, both are semi-unitary matrices. $\mathbf{Q}_1 \in \mathbb{C}^{N_s \times N_s}$ is an upper triangular matrix, while $*$ is an arbitrary matrix which can be neglected. The largest N_s singular values are formulated as $q_{i,i} = (\delta_1, \delta_2, ..., \delta_{N_s})^{\frac{1}{N_s}} \in \bar{\mathbf{q}}, \forall i$, where $q_{i,j}$ represents the elements in matrix $\mathbf{Q}_1$. The received signal is given as

$$\begin{aligned} \mathbf{y} &= \mathbf{B}^H \mathbf{H} \mathbf{x} + \mathbf{B}^H \mathbf{n} \\ &= \mathbf{W}_1^H \mathbf{H} \mathbf{R}_1 \mathbf{s} + \mathbf{W}_1^H \mathbf{n} \\ &= \mathbf{Q}_1 \mathbf{s} + \mathbf{W}_1^H \mathbf{n}. \end{aligned} \tag{31}$$

The loss function is given as

$$\begin{aligned} loss &= \|\mathbf{R}_1 - \mathbf{R}_A \mathbf{R}_D\|_F \\ &= \sqrt{\text{tr}((\mathbf{R}_1 - \mathbf{R}_A \mathbf{R}_D)(\mathbf{R}_1 - \mathbf{R}_A \mathbf{R}_D)^H)} \\ &= \sqrt{\textstyle\sum_{i=1}^{\min\{N_t, N_s\}} \delta_i^2 (\mathbf{R}_1 - \mathbf{R}_A \mathbf{R}_D)}, \end{aligned} \tag{32}$$

where $\|\cdot\|$ represents the Frobenious norm, $\mathbf{R}_A$ and $\mathbf{R}_D$ represent the GMD-based analog and digital precoder, respectively. In addition, $\delta_i(\mathbf{R}_1 - \mathbf{R}_A \mathbf{R}_D)$ represent the singular values of matrix

$(\mathbf{R}_1 - \mathbf{R}_A\mathbf{R}_D)$. In (32), the constraints $|\{\mathbf{R}_A\}_{i,j}| = \frac{1}{\sqrt{N_t}}$ and tr$(\mathbf{R}_A\mathbf{R}_D)\mathbf{R}_D^H\mathbf{R}_A^H \leq N_s$ need to be satisfied. To construct an autoencoder, the DNN framework is employed as

$$\mathbf{R}_1 = f(\mathbf{R}_A\mathbf{R}_D; \Omega), \tag{33}$$

where Ω represent the dataset of the samples and $f(\cdot)$ represent the mapping relation for which, the detailed training procedure is provided as follows.

The proposed DL-based scheme is considered as a mapping operation and a training mechanism is formulated for extracting the structural statistics of the mm-Wave-based model. Th matrices $\mathbf{R}_A$ and $\mathbf{R}_D$ are initialized as empty matrices after which the random data sequences is generated in the DNN. The DNN is trained with the input data sequences as per different channel conditions and $\mathbf{R}_A$ and $\mathbf{R}_D$ is updated. Correspondingly, the physical AoA θ_p^r and AoD θ_p^t is generated randomly and the bias between $\mathbf{R}_1$ and $\mathbf{R}_A\mathbf{R}_D$ is obtained from the output layer of the DNN. The bias obtained is based on the input signals in different cases through a large number of iterations. Thus, the training set Ω is achieved which consists the structural feature of the mm-Wave massive MIMO model and the input data sequences and output data of the DNN. This is a unsupervised learning training approach. Next, the DNN needs to be tested after being trained thoroughly. Based on the given input signal vectors without any iterations, the analog precoder $\mathbf{R}_A$ and the digital precoder $\mathbf{R}_D$ is obtained for each channel condition. The stochastic gradient descent (SGD) algorithm with momentum is employed to process the loss function given as

$$\mathbf{R}_A^{j+1} = \mathbf{R}_A^j + v, \tag{34}$$

$$\mathbf{R}_D^{j+1} = \mathbf{R}_D^j + v, \tag{35}$$

where v represents the velocity for facilitating the gradient element and j represents the iteration. $\mathbf{R}_A^0$ and $\mathbf{R}_D^0$ are assumed to be the randomly generated initial solutions for $\mathbf{R}_A$ and $\mathbf{R}_D$,

respectively. The update procedure of v can be given as

$$\begin{aligned} v &= \alpha v - \epsilon g \\ &= \alpha v - \epsilon \frac{1}{N} \nabla_{\mathbf{R}_A, \mathbf{R}_D} \sqrt{\sum_{i=1}^{\min\{N_t, N_s\}} \delta_i^2 (\mathbf{R}_1 - \mathbf{R}_A \mathbf{R}_D)}, \end{aligned} \tag{36}$$

where α represents the momentum parameter and ϵ represents the learning rate. Also, g and N represent the gradient element and the number of samples, respectively. The learning framework for hybrid precoding is described in **Algorithm 3**.

5.3 Numerical Results

In this section, the performance of the proposed DNN-based mm-Wave massive MIMO scheme is presented. Without loss of generality, the mm-Wave channel model has been generated [28] and to construct and process the DNN framework, *Keras* is used. In addition, $P = 3$ and the carrier frequency is considered as 28 GHz. The bit-error ratio (BER) performance is evaluated with different learning rates and the network has been trained for $45k$ iterations in simulation.

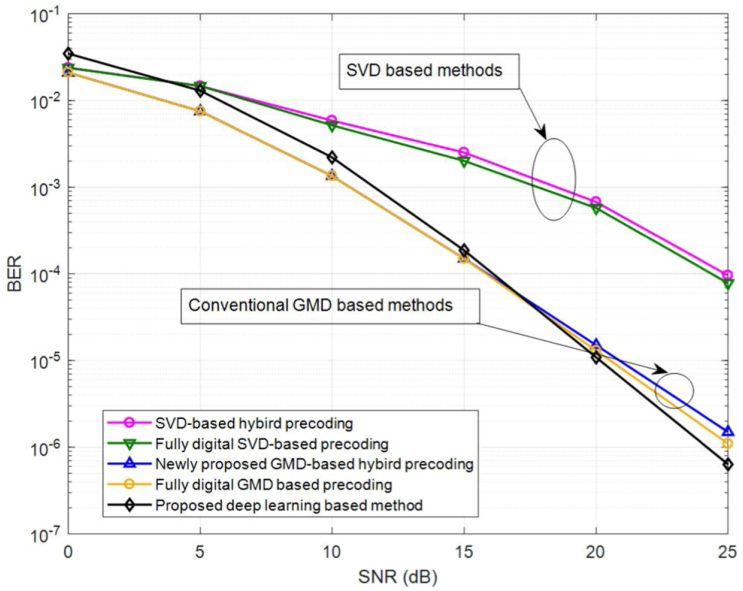

Figure 8: BER versus SNR in the case of the proposed DNN-based, SVD-based hybrid precoding scheme [3] and other conventional schemes

The BER performance of the DNN-based proposed scheme is compared with the BER of SVD-based hybrid precoding scheme [3], fully digital SVD-based precoding scheme, full GMD-

based precoding scheme and the new GMD-based precoding scheme [26]. In Fig. 8 [2], the BER is calculated againt the SNR for the the DL-based precoding scheme and the above-mentioned precoding schemes and it can be seen that DL-based method outperforms other conventional precoding schemes. This establishes the excellent representation ability of DL. The DNN exploits the structural information of the mm-Wave massive MIMO system and approaches each iteration of the hybrid precoding algorithm. This verifies the superiority of the proposed scheme over fully GMD-based digital precoding scheme which, in turn, implies that the DL can be useful in solving the existing non-convex optimization problem in hybrid precoding.

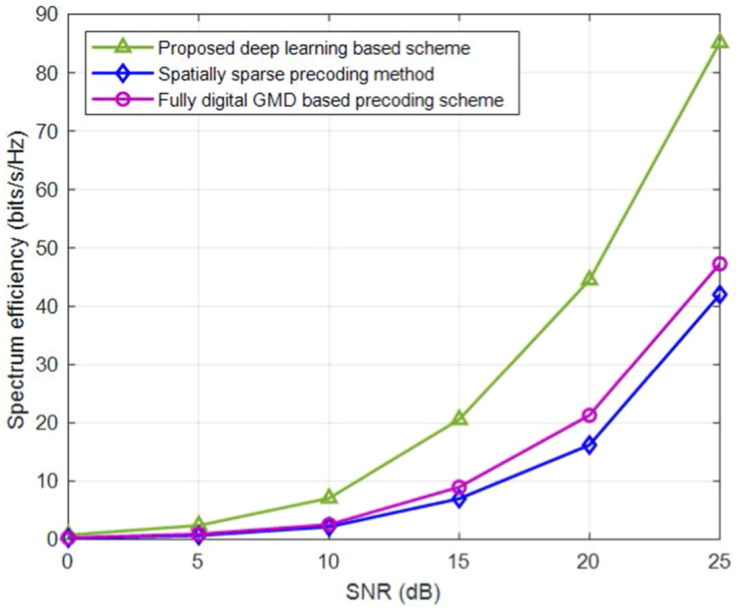

Figure 9: Spectrum efficiency versus SNR in the case of the proposed deep learning based hybrid precoding scheme, the spatially sparse precoding method [3], and the fully digital GMD based precoding scheme.

In Fig. 9 [2], the spectrum efficiency against the SNR is shown for the proposed DL-based hybrid precoding scheme, the spatially sparse precoding scheme [3] and the fully digital GMD-based precoding scheme. From Fig. 9, it can be observed that the proposed DL-based hybrid precoding scheme again achieves better performance compared to other schemes. This shows the outstanding mapping and learning capabilities of the DL. Additionally, when the SNR increases, the performance gap of the DL-based scheme and the other schemes becomes larger, implying the further superiority of the proposed DL-based hybrid precoding scheme.

6 Complexity Analysis

Table 1: Complexity comparison

	Number of Multiplications	**Number of Divisions**
DL-based scheme [2]	$\mathcal{O}(N_s N_t^2)$	$\mathcal{O}(L^2)$
SIC-based hybrid precoding [1]	$\mathcal{O}(N_t^2(N_s N_r + K))$	$\mathcal{O}(2N_r N_s)$
Spatially sparse precoding [3]	$\mathcal{O}(N_r^4 N_t + N_r^2 L^2 + N_r^2 N_t^2 L)$	$\mathcal{O}(2N_r^3)$

The computational complexity of the SIC-based hybrid precodings cheme and DL-scheme is illustrated in Table 1 which are compared with computational complexity of the SVD-based hybrid precoding scheme [3]. For simplicity of the notations in all three works, let us assume that N_s independent input data streams are transmitted by N_t transmit antennas through L effective channel paths to K users, each with N_r receive antennas.

The advantage of the proposed hybrid precoding scheme is that it has the lowest computational complexity compared to the SIC-based hybrid precoding [1] and SVD-based hybrid precoding [3].

7 Critical Review and Future Work

The basic idea of SIC-based hybrid precoding can be summarized as follows: (1) it decomposes the total achievable rate optimization problem with nonconvex constraints into a series of simple subrate optimization problems, each of which only considers one subantenna array; (2) it proves that maximizing the achievable subrate of each subantenna array is equivalent to simply seeking a precoding vector sufficiently close (in terms of Euclidean distance) to the unconstrained optimal solution; and (3) it maximizes the achievable subrate of each subantenna array one by one until the last subantenna array is considered. Simulation results verify that SIC-based hybrid precoding is near optimal and enjoys higher energy efficiency than the spa- tially sparse precoding and the fully digital precoding.

This report has reviewed two different approaches, both of which are addressing the same problem of hybrid precoding and presented different methods and low-complexity solutions for the non-convex optimization problem to achieve near-optimal solutions. However, these methods are less-complex than the conventional SVD and GMD-based methods, there are still some issues which are given as

1. In the first paper [1], the analysis of mm-Wave system is focussed for narrowband, whereas mm-Wave signals, due to it's large unused bandwidth can be considered for broadband [29].

2. The results are focussed to maximize the total achievable rate of mm-Wave MIMO systems, whereas the maximization sum-rate criterion can also suppress the interference as much as possible, and the mathematical quantification of such interference will be an important topic for future work.

3. In addition, the characteristics of mm-Wave systems (e.g., channel sparsity) should be efficiently exploited in the design of compensation algorithms by taking into account the large- scale antenna arrays and wide bandwidth. [30]

4. In conventional fully digital precoding, the extension from the narrowband to the wide-band channel is straightforward by utilizing the orthogonal frequency division multiplexing

(OFDM). It converts the frequency-selective wideband channel to a series of frequency-flat subchannels. However, it cannot work for hybrid precoding, where the subcarrier-dependent digital precoder is designed in the frequency domain, while the subcarrier-independent analog precoder realized by the PSs is designed in the time domain which is common across all the subcarriers. This unique characteristic of frequency-selective hybrid precoding differentiates it from the traditional fully-digital precoding and makes it more challenging in the wideband mm-Wave channels.[31]

5. Nevertheless, lens-based antenna arrays still suffer from manufacturing imperfections, while their physical dimensions are inherently large. The loss of focus in lens-based antenna arrays, due to the limited number of arranged feeders around the lens, is also a great challenge.

   The focus loss of lens topologies can be alleviated by the combined use of lens and PSs, where the lens is used for beamforming, while the phase shifters are used for multiple adjacent beams combination.

6. Mm-Wave encountered hardware constraints contain the ultra-high data processing pressure and the imperfections resulting from the components of the wideband beamforming hardware, for example, phase shifters and lens arrays. Moreover, low-power and low-cost design is also a great challenge in future mm-Wave system architecture.

   Regarding the stringent high data processing requirements, using low-resolution ADCs in hardware combined with advanced receiver algo- rithms, for example, the generalized expectation consistent (GEC) signal recovery algorithm [12], emerges as a viable candidate.

7. However, it is still difficult to establish a general framework embracing all these hardware constraints and imperfections. Most importantly, it is immensely difficult to achieve optimal performance for the entire system by optimizing different modules separately.

8. To overcome the large path loss, mm-Wave systems are typically configured with large-scale antenna arrays at the base station. Hence, exploiting advanced array signal processing in mm-Wave systems is important for the purpose of reducing signal processing

complexity and, at the same time, achieving enhanced performance. Particularly, the inherent array structure of massive antennas in mm-Wave systems could be re-conceptualized and explored from the array signal processing view-point, for example, direction of arrival/departure and beam squint, which can then be applied in mm-Wave system operation design, such as channel estimation, hybrid beamforming, interference control, multiple access scheme, and mobility management via angle tracking.

9. By using the training dataset (pre-obtained or online) to learn the actual signal model and refine the parameters of algorithms via DL, mm-Wave systems may be able to overcome hardware constraints and imperfections in terms of signal processing algorithms.

10. The joint optimal design of Digital precoder matrix D and Analog precoder matrix A is still an open issue [32].

11. Techniques for efficient mm-Wave channel estimation that potentially leverage the geometric nature of mm-Wave channels [55]–[57], as well as the rigorous treatment of frequency selectivity, are still an ongoing topic of research [3].

12. What is the performance gap compared to digital BF?

13. Does a larger transceiver number N always lead to better EE, and what is the EE-SE optimal design?

14. How can we design efficient reference signals (RSs) for better availability of the channel state information at the transmitter side? [32]

8 Conclusion

In this report, we have discussed the hybrid precoding techniques in mm-Wave massive MIMO systems. The need of energy-efficient less-complex solutions to solve non-convex problems in hybrid precoding inspires us to use different methods and approaches. Deep learning is a promising technique and has been successfully applied to improve the performance of baseband signal processing algorithms including channel decoding, channel estimation and detection, and so on.

Therefore, to achieve better performance in mm-Wave systems, considering the difficulties and complexities of deducing an accurate analytical signal model that embraces all the hardware constraints and imperfections, it could be more practical and of great benefit to leverage DL.

References

[1] X. Gao, L. Dai, S. Han, I. Chih-Lin, and R. W. Heath, "Energy-efficient hybrid analog and digital precoding for mmwave mimo systems with large antenna arrays," *IEEE Journal on Selected Areas in Communications*, vol. 34, no. 4, pp. 998–1009, 2016.

[2] H. Huang, Y. Song, J. Yang, G. Gui, and F. Adachi, "Deep-learning-based millimeter-wave massive mimo for hybrid precoding," *IEEE Transactions on Vehicular Technology*, vol. 68, no. 3, pp. 3027–3032, 2019.

[3] O. El Ayach, S. Rajagopal, S. Abu-Surra, Z. Pi, and R. W. Heath, "Spatially sparse precoding in millimeter wave mimo systems," *IEEE transactions on wireless communications*, vol. 13, no. 3, pp. 1499–1513, 2014.

[4] S. A. Busari, K. M. S. Huq, S. Mumtaz, L. Dai, and J. Rodriguez, "Millimeter-wave massive mimo communication for future wireless systems: A survey," *IEEE Communications Surveys & Tutorials*, vol. 20, no. 2, pp. 836–869, 2017.

[5] F. Khan and Z. Pi, "mmwave mobile broadband (mmb): Unleashing the 3–300ghz spectrum," in *34th IEEE Sarnoff Symposium*. IEEE, 2011, pp. 1–6.

[6] Z. Shi, R. Lu, J. Chen, and X. S. Shen, "Three-dimensional spatial multiplexing for directional millimeter-wave communications in multi-cubicle office environments," in *2013 IEEE Global Communications Conference (GLOBECOM)*. IEEE, 2013, pp. 4384–4389.

[7] S. Mumtaz, J. Rodriguez, and L. Dai, *MmWave Massive MIMO: A Paradigm for 5G*. Academic Press, 2016.

[8] L. Dai, B. Wang, M. Peng, and S. Chen, "Hybrid precoding-based millimeter-wave massive mimo-noma with simultaneous wireless information and power transfer," *IEEE Journal on Selected Areas in Communications*, vol. 37, no. 1, pp. 131–141, 2018.

[9] A. Alkhateeb, J. Mo, N. Gonzalez-Prelcic, and R. W. Heath, "Mimo precoding and combining solutions for millimeter-wave systems," *IEEE Communications Magazine*, vol. 52, no. 12, pp. 122–131, 2014.

[10] S. Hur, T. Kim, D. J. Love, J. V. Krogmeier, T. A. Thomas, and A. Ghosh, "Millimeter wave beamforming for wireless backhaul and access in small cell networks," *IEEE Transactions on Communications*, vol. 61, no. 10, pp. 4391–4403, 2013.

[11] Y.-Y. Lee, C.-H. Wang, and Y.-H. Huang, "A hybrid rf/baseband precoding processor based on parallel-index-selection matrix-inversion-bypass simultaneous orthogonal matching pursuit for millimeter wave mimo systems," *IEEE Transactions on Signal Processing*, vol. 63, no. 2, pp. 305–317, 2014.

[12] A. Alkhateeb, G. Leus, and R. W. Heath, "Limited feedback hybrid precoding for multi-user millimeter wave systems," *IEEE transactions on wireless communications*, vol. 14, no. 11, pp. 6481–6494, 2015.

[13] A. Alkhateeb, O. El Ayach, G. Leus, and R. W. Heath, "Channel estimation and hybrid precoding for millimeter wave cellular systems," *IEEE Journal of Selected Topics in Signal Processing*, vol. 8, no. 5, pp. 831–846, 2014.

[14] Y. LeCun, Y. Bengio, and G. Hinton, "Deep learning. nature 521," 2015.

[15] D. Yu and L. Deng, "Deep learning and its applications to signal and information processing [exploratory dsp]," *IEEE Signal Processing Magazine*, vol. 28, no. 1, pp. 145–154, 2010.

[16] I. Goodfellow, Y. Bengio, and A. Courville, *Deep learning*. MIT press, 2016.

[17] D. E. Rumelhart, G. E. Hinton, and R. J. Williams, "Learning representations by back-propagating errors," *nature*, vol. 323, no. 6088, pp. 533–536, 1986.

[18] S. Hochreiter and J. Schmidhuber, "Long short-term memory," *Neural computation*, vol. 9, no. 8, pp. 1735–1780, 1997.

[19] G. E. Hinton, S. Osindero, and Y.-W. Teh, "A fast learning algorithm for deep belief nets," *Neural computation*, vol. 18, no. 7, pp. 1527–1554, 2006.

[20] M. Ranzato, C. Poultney, S. Chopra, and Y. L. Cun, "Efficient learning of sparse representations with an energy-based model," in *Advances in neural information processing systems*, 2007, pp. 1137–1144.

[21] C. Van Loan and G. Golub, "Matrix computations, vol. 3," 2012.

[22] Å. Björck, *Numerical methods in matrix computations*. Springer, 2015, vol. 59.

[23] O. El Ayach, R. W. Heath, S. Rajagopal, and Z. Pi, "Multimode precoding in millimeter wave mimo transmitters with multiple antenna sub-arrays," in *2013 IEEE Global Communications Conference (GLOBECOM)*. IEEE, 2013, pp. 3476–3480.

[24] W. Roh, J.-Y. Seol, J. Park, B. Lee, J. Lee, Y. Kim, J. Cho, K. Cheun, and F. Aryanfar, "Millimeter-wave beamforming as an enabling technology for 5g cellular communications: Theoretical feasibility and prototype results," *IEEE communications magazine*, vol. 52, no. 2, pp. 106–113, 2014.

[25] F. Rusek, D. Persson, B. K. Lau, E. G. Larsson, T. L. Marzetta, O. Edfors, and F. Tufvesson, "Scaling up mimo: Opportunities and challenges with very large arrays," *IEEE Signal Processing Magazine*, vol. 30, no. 1, pp. 40–60, 2013.

[26] T. Xie, L. Dai, X. Gao, M. Z. Shakir, and J. Li, "Geometric mean decomposition based hybrid precoding for millimeter-wave massive mimo," *China Communications*, vol. 15, no. 5, pp. 229–238, 2018.

[27] K. Hornik, M. Stinchcombe, and H. White, "Multilayer feedforward networks are universal approximators," *Neural networks*, vol. 2, no. 5, pp. 359–366, 1989.

[28] A. Ghosh, T. A. Thomas, M. C. Cudak, R. Ratasuk, P. Moorut, F. W. Vook, T. S. Rappaport, G. R. MacCartney, S. Sun, and S. Nie, "Millimeter-wave enhanced local area systems: A high-data-rate approach for future wireless networks," *IEEE Journal on Selected Areas in Communications*, vol. 32, no. 6, pp. 1152–1163, 2014.

[29] Z. Pi and F. Khan, "An introduction to millimeter-wave mobile broadband systems," *IEEE Communications Magazine*, vol. 49, no. 6, pp. 101–107, June 2011.

[30] X. Yang, M. Matthaiou, J. Yang, C.-K. Wen, F. Gao, and S. Jin, "Hardware-constrained millimeter-wave systems for 5g: Challenges, opportunities, and solutions," *IEEE Communications Magazine*, vol. 57, no. 1, pp. 44–50, 2019.

[31] T. Mir, M. Z. Siddiqi, U. Mir, R. Mackenzie, and M. Hao, "Machine learning inspired hybrid precoding for wideband millimeter-wave massive mimo systems," *IEEE Access*, vol. 7, pp. 62 852–62 864, 2019.

[32] S. Han, I. Chih-Lin, Z. Xu, and C. Rowell, "Large-scale antenna systems with hybrid analog and digital beamforming for millimeter wave 5g," *IEEE Communications Magazine*, vol. 53, no. 1, pp. 186–194, 2015.

[33] D. Tse and P. Viswanath, *Fundamentals of wireless communication*. Cambridge university press, 2005.

Appendix

Algorithm 1: Power iteration algorithm

Input : (1) $\bar{\mathbf{G}}_{n-1}$
(2) Initial solution $\mathbf{u}^{(0)}$;
(3) maximum number of iteration S

for $1 \leq s \leq S$ **do**
  1) $\mathbf{z}^{(s)} = \bar{\mathbf{G}}_{n-1}\mathbf{u}^{(s-1)}$
  2) $m^{(s)} = \arg\max_{z_i^{(s)}} \left| z_i^{(s)} \right|$
  3)
  if $1 \leq s \leq 2$
    $n^{(s)} = m^{(s)}$
  else
    $n^{(s)} = \frac{m^{(s)}m^{(s-2)} - (m^{(s-1)})^2}{m^{(s)} - 2m^{(s-1)} + m^{(s-2)}}$
  end
  4) $\mathbf{u}^{(s)} = \frac{\mathbf{z}^{(s)}}{n^{(s)}}$
end

Output: (1) The largest singular value $\Sigma_1 = n^{(S)}$
(2) The first singular vector $\mathbf{v}_1 = \frac{\mathbf{u}^{(S)}}{\left\|\mathbf{u}^{(S)}\right\|_2}$

Algorithm 2: SIC-based hybrid precoding

Input : $\bar{\mathbf{G}}_0$

for $1 \leq n \leq N$ **do**
  1) Compute $\mathbf{v}_1$ and Σ_1 of $\bar{\mathbf{G}}_{n-1}$ by **Algorithm 1**
  2) $\bar{\mathbf{a}}_n^{\text{opt}} = \frac{1}{\sqrt{M}} e^{j\text{angle}(\mathbf{v}_1)}$, $d_n^{\text{opt}} = \frac{\|\mathbf{v}_1\|_1}{\sqrt{M}}$,
    $\bar{\mathbf{p}}_n^{\text{opt}} = \frac{1}{M}\|\mathbf{v}_1\|_1 e^{j\text{angle}(\mathbf{v}_1)}$ (15)-(17)
  3) $\bar{\mathbf{G}}_n = \bar{\mathbf{G}}_{n-1} - \frac{\frac{\rho}{N\sigma^2}\Sigma_1^2 \mathbf{v}_1\mathbf{v}_1^H}{1+\frac{\rho}{N\sigma^2}\Sigma_1}$ **(Proposition 2)**
end

Output: (1) $\mathbf{D} = \text{diag}\{d_1^{\text{opt}}, \ldots, d_N^{\text{opt}}\}$
(2) $\mathbf{A} = \text{diag}\{\bar{\mathbf{a}}_1^{\text{opt}}, \ldots, \bar{\mathbf{a}}_N^{\text{opt}}\}$
(3) $\mathbf{P} = \mathbf{AD}$

1. Proof of ***Proposition 1***: The target optimization problem (11) can be defined as

$$R_n = \log_2\Big(1 + \frac{\rho}{N\sigma^2}\bar{\mathbf{p}}_n^H \bar{\mathbf{G}}_{n-1}\bar{\mathbf{p}}_n\Big), \tag{37}$$

and the SVD of $\bar{\mathbf{G}}_{n-1}$ as $\bar{\mathbf{G}}_{\boldsymbol{n-1}} = \mathbf{V}\boldsymbol{\Sigma}\mathbf{V}^{\boldsymbol{H}}$. By separating the matrices $\boldsymbol{\Sigma}$ and $\mathbf{V}$ into two

Algorithm 3: DNN-based hybrid precoding

Input : The physical AoA θ_p^r and AoD θ_p^t, environment simulator.
Output: Optimized precoder $\mathbf{R}_1$.

Initialization: The amount of iteration is initialized as $j = 0$ and the weight is $\omega = 0$. Meanwhile, initialize error threshold as $\tau = 10^{-7}$. Furthermore, set $\mathbf{R}_A = \mathbf{0}$ and $\mathbf{R}_D = \mathbf{0}$.
Product a series of training sequences. Also, θ_p^r and θ_p^t are generated randomly.
Construct the proposed DNN framework.
Process the environment simulator to simulate wireless channel with noise.
while *error* $\geq \tau$
    Train the DNN by processing the SGD with momentum according to (34), (35), (36).
    Update $\mathbf{R}_A$ and $\mathbf{R}_D$.
    Obtain the bias between $\mathbf{R}_1$ and $\mathbf{R}_A\mathbf{R}_D$ from the output layer of this network.
end
return: Optimized precoder $\mathbf{R}_1$.

parts as

$$\mathbf{\Sigma} = \begin{bmatrix} \Sigma_1 & 0 \\ 0 & \mathbf{\Sigma_2} \end{bmatrix}, \quad \mathbf{V} = [\mathbf{v}_1 \ \mathbf{V}_2] \tag{38}$$

R_n in (37) is rewritten as

$$\begin{aligned} R_n &= \log_2\Big(1 + \frac{\rho}{N\sigma^2}\bar{\mathbf{p}}_n^H \bar{\mathbf{G}}_{n-1}\bar{\mathbf{p}}_n\Big), \\ &= \log_2\Big(1 + \frac{\rho}{N\sigma^2}\bar{\mathbf{p}}_n^H \mathbf{V}\mathbf{\Sigma}\mathbf{V}^H\bar{\mathbf{p}}_n\Big) \\ &= \log_2\Big(1 + \frac{\rho}{N\sigma^2} \times \bar{\mathbf{p}}_n^H[\mathbf{v}_1\mathbf{V}_2]\begin{bmatrix} \Sigma_1 & 0 \\ 0 & \mathbf{\Sigma_2} \end{bmatrix}[\mathbf{v}_1\mathbf{V}_2]^T\bar{\mathbf{p}}_n\Big), \\ &= \log_2\Big(1 + \frac{\rho}{N\sigma^2}\bar{\mathbf{p}}_n^H \mathbf{v}_1\Sigma_1\mathbf{v}_1^H\bar{\mathbf{p}}_n + \frac{\rho}{N\sigma^2}\bar{\mathbf{p}}_n^H \mathbf{V}_2\mathbf{\Sigma_2}\mathbf{V}_2^H\bar{\mathbf{p}}_n\Big). \end{aligned} \tag{39}$$

It is assumed that $\bar{\mathbf{p}_n}$ is approximately orthogonal to the matrix $\mathbf{V}_2$, i.e., $\bar{\mathbf{p}}_n^H\mathbf{V}_2 \approx 0$ [3]. Hence, (39) is simplified as

$$\begin{aligned} R_n &\approx \log_2\Big(1 + \frac{\rho\Sigma_1}{N\sigma^2}\bar{\mathbf{p}}_n^H \mathbf{v}_1\mathbf{v}_1^H\bar{\mathbf{p}}_n\Big) \\ &\overset{(a)}{=} \log_2\Big(1 + \frac{\rho\Sigma_1}{N\sigma^2}\Big) + \log_2\Big(1 - \Big(1 + \frac{\rho\Sigma_1}{N\sigma^2}\Big)^{-1}\frac{\rho\Sigma_1}{N\sigma^2}(1 - \bar{\mathbf{p}}_n^H \mathbf{v}_1\mathbf{v}_1^H\bar{\mathbf{p}}_n)\Big) \\ &\overset{(b)}{\approx} \log_2\Big(1 + \frac{\rho\Sigma_1}{N\sigma^2}\Big) + \log_2(\bar{\mathbf{p}}_n^H \mathbf{v}_1\mathbf{v}_1^H\bar{\mathbf{p}}_n)) \end{aligned} \tag{40}$$

where (a) is obtained by using the formula $\mathbf{I} + \mathbf{XY} = (\mathbf{I} + \mathbf{X})(\mathbf{I} - (\mathbf{I} + \mathbf{X})^{-1}\mathbf{X}(\mathbf{I} - \mathbf{Y}))$

[3], and the terms are defined as $\mathbf{X} = \frac{\rho\Sigma_1}{N\sigma^2}$ and $\mathbf{Y} = \bar{\mathbf{p}}_n^H \mathbf{v}_1 \mathbf{v}_1^H \bar{\mathbf{p}}_n$; (b) is valid for high SNR approximation [33], i.e.,

$$\left(1 + \frac{\rho\Sigma_1}{N\sigma^2}\right)^{-1} \frac{\rho\Sigma_1}{N\sigma^2} \approx 1. \tag{41}$$

From (40), it can be observed that maximizing R_n is equivalent to maximizing $\bar{\mathbf{p}}_n^H \mathbf{v}_1 \mathbf{v}_1^H \bar{\mathbf{p}}_n = \left\|\bar{\mathbf{p}}_n^H \mathbf{v}_1\right\|_2^2$. The largest projection of vector $\bar{\mathbf{p}}_n$, leads to the smallest Euclidean distance to $\mathbf{v}_1$ and based on this, the optimization problem (11) is equivalent to the following optimization problem

$$\bar{\mathbf{p}}_n^{\text{opt}} = \underset{\bar{\mathbf{p}}_n \in \bar{\mathcal{F}}}{\arg\min} \|\mathbf{v}_1 - \bar{\mathbf{p}}_n\|_2^2 . \tag{42}$$

2. Proof of ***Proposition 2***: To compute $\bar{\mathbf{G}}_n$ (12), the matrix $\mathbf{T}_n = \mathbf{I}_K + \frac{\rho}{N\sigma^2}\mathbf{H}\mathbf{P}_n\mathbf{P}_n^H\mathbf{H}^H$ is inversed. By partitioning $\mathbf{P}_n$ as $\mathbf{P}_n = [\mathbf{P}_{n-1}\mathbf{p}_n]$, $\mathbf{T}_n$ can be rewritten as

$$\begin{aligned}
\mathbf{T}_n &= \mathbf{I}_K + \frac{\rho}{N\sigma^2}\mathbf{H}\mathbf{P}_n\mathbf{P}_n^H\mathbf{H}^H \\
&= \mathbf{I}_K + \frac{\rho}{N\sigma^2}\mathbf{H}[\mathbf{P}_{n-1}\mathbf{p}_n][\mathbf{P}_{n-1}\mathbf{p}_n]^H\mathbf{H}^H \\
&= \mathbf{I}_K + \frac{\rho}{N\sigma^2}\mathbf{H}\mathbf{P}_{n-1}\mathbf{P}_{n-1}^H\mathbf{H}^H + \frac{\rho}{N\sigma^2}\mathbf{H}\mathbf{p}_n\mathbf{p}_n^H\mathbf{H}^H \\
&= \mathbf{T}_{n-1} + \frac{\rho}{N\sigma^2}\mathbf{H}\mathbf{p}_n\mathbf{p}_n^H\mathbf{H}^H.
\end{aligned} \tag{43}$$

Then, by utilizing the Shermon-Morrison formula [[21], Eq 2.1.4]

$$\left(\mathbf{A} + \mathbf{u}\mathbf{v}^T\right)^{-1} = \mathbf{A}^{-1} - \frac{\mathbf{A}^{-1}\mathbf{u}\mathbf{v}^T\mathbf{A}^{-1}}{1 + \mathbf{v}^T\mathbf{A}^{-1}\mathbf{u}} \tag{44}$$

$\mathbf{T}_n^{-1}$ can be represented as

$$\begin{aligned}
\mathbf{T}_n^{-1} &= \left(\mathbf{T}_{n-1} + \frac{\rho}{N\sigma^2}\mathbf{H}\mathbf{p}_n\mathbf{p}_n^H\mathbf{H}^H\right)^{-1} \\
&= \mathbf{T}_{n-1}^{-1} - \frac{\frac{\rho}{N\sigma^2}\mathbf{T}_{n-1}^{-1}\mathbf{H}\mathbf{p}_n\mathbf{p}_n^H\mathbf{H}^H\mathbf{T}_{n-1}^{-1}}{1 + \frac{\rho}{N\sigma^2}\mathbf{p}_n^H\mathbf{H}^H\mathbf{T}_{n-1}^{-1}\mathbf{H}\mathbf{p}_n}.
\end{aligned} \tag{45}$$

Substituting (45) into $\bar{\mathbf{G}}_n = \mathbf{H}^H \mathbf{T}_{n-1}^{-1} \mathbf{H}$, $\bar{\mathbf{G}}_n$ is given as

$$\begin{aligned}
\bar{\mathbf{G}}_n &= \mathbf{H}^H \mathbf{T}_{n-1}^{-1} \mathbf{H} \\
&= \mathbf{H}^H \left(\mathbf{T}_{n-1}^{-1} - \frac{\frac{\rho}{N\sigma^2} \mathbf{T}_{n-1}^{-1} \mathbf{H} \mathbf{p}_n \mathbf{p}_n^H \mathbf{H}^H \mathbf{T}_{n-1}^{-1}}{1 + \frac{\rho}{N\sigma^2} \mathbf{p}_n^H \mathbf{H}^H \mathbf{T}_{n-1}^{-1} \mathbf{H} \mathbf{p}_n} \right) \mathbf{H} \\
&= \mathbf{G}_{n-1} - \frac{\frac{\rho}{N\sigma^2} \mathbf{G}_{n-1} \mathbf{p}_n \mathbf{p}_n^H \mathbf{G}_{n-1}}{1 + \frac{\rho}{N\sigma^2} \mathbf{p}_n^H \mathbf{G}_{n-1} \mathbf{p}_n}
\end{aligned} \tag{46}$$

Then, according to (12), $\bar{\mathbf{G}_n}$ can be obtained by

$$\begin{aligned}
\bar{\mathbf{G}_n} &= \mathbf{R} \mathbf{G}_n \mathbf{R}^H \\
&= \mathbf{R} \left(\mathbf{G}_{n-1} - \frac{\frac{\rho}{N\sigma^2} \mathbf{G}_{n-1} \mathbf{p}_n \mathbf{p}_n^H \mathbf{G}_{n-1}}{1 + \frac{\rho}{N\sigma^2} \mathbf{p}_n^H \mathbf{G}_{n-1} \mathbf{p}_n} \right) \mathbf{R}^H \\
&= \left(\bar{\mathbf{G}}_{n-1} - \frac{\frac{\rho}{N\sigma^2} \bar{\mathbf{G}}_{n-1} \bar{\mathbf{p}}_n \bar{\mathbf{p}}_n^H \bar{\mathbf{G}}_{n-1}}{1 + \frac{\rho}{N\sigma^2} \bar{\mathbf{p}}_n^H \bar{\mathbf{G}}_{n-1} \bar{\mathbf{p}}_n} \right).
\end{aligned} \tag{47}$$

In Section 4.2.1, the precoding vector $\bar{\mathbf{p}}_n$ is obtained sufficiently close t $\mathbf{v}_1$, i.e., $\bar{\mathbf{p}}_n \approx \mathbf{v}_1$. Then, (47) can be well approximated by replacing $\bar{\mathbf{p}}_n$ with $\mathbf{v}_1$ as

$$\begin{aligned}
\bar{\mathbf{G}_n} &= \bar{\mathbf{G}}_{n-1} - \frac{\frac{\rho}{N\sigma^2} \bar{\mathbf{G}}_{n-1} \bar{\mathbf{p}}_n \bar{\mathbf{p}}_n^H \bar{\mathbf{G}}_{n-1}}{1 + \frac{\rho}{N\sigma^2} \bar{\mathbf{p}}_n^H \bar{\mathbf{G}}_{n-1} \bar{\mathbf{p}}_n} \\
&\approx \bar{\mathbf{G}}_{n-1} - \frac{\frac{\rho}{N\sigma^2} \bar{\mathbf{G}}_{n-1} \mathbf{v}_1 \mathbf{v}_1^H \bar{\mathbf{G}}_{n-1}}{1 + \frac{\rho}{N\sigma^2} \mathbf{v}_1^H \bar{\mathbf{G}}_{n-1} \mathbf{v}_1} \\
&\overset{(a)}{=} \bar{\mathbf{G}}_{n-1} - \frac{\frac{\rho}{N\sigma^2} \Sigma_1^2 \mathbf{v}_1 \mathbf{v}_1^H}{1 + \frac{\rho}{N\sigma^2} \Sigma_1},
\end{aligned} \tag{48}$$

where (a) is true due to the fact that $\mathbf{v}_1^H \bar{\mathbf{G}}_{n-1} = \Sigma_1 \mathbf{v}_1^H$, since $\bar{\mathbf{G}}_{n-1}$ is an Hermitian matrix.